



HAL
open science

Alteration of potash-lime silicate glass in atmospheric medium: study of mechanisms and kinetics using ^{18}O and D isotopes

Loryelle Sessegolo, Aurélie Verney-Carron, Nathalie Valle, Patrick Ausset, Sathya Narayanasamy, Sophie Nowak, Chloé Fourdrin, Mandana Saheb, Anne Chabas

► To cite this version:

Loryelle Sessegolo, Aurélie Verney-Carron, Nathalie Valle, Patrick Ausset, Sathya Narayanasamy, et al.. Alteration of potash-lime silicate glass in atmospheric medium: study of mechanisms and kinetics using ^{18}O and D isotopes. *Journal of Non-Crystalline Solids*, 2021, 570, 10.1016/j.jnoncrysol.2021.121020 . insu-03749613

HAL Id: insu-03749613

<https://insu.hal.science/insu-03749613>

Submitted on 2 Aug 2023

HAL is a multi-disciplinary open access archive for the deposit and dissemination of scientific research documents, whether they are published or not. The documents may come from teaching and research institutions in France or abroad, or from public or private research centers.

L'archive ouverte pluridisciplinaire **HAL**, est destinée au dépôt et à la diffusion de documents scientifiques de niveau recherche, publiés ou non, émanant des établissements d'enseignement et de recherche français ou étrangers, des laboratoires publics ou privés.



Distributed under a Creative Commons Attribution - NonCommercial 4.0 International License

Alteration of potash-lime silicate glass in atmospheric medium: study of mechanisms and kinetics using ^{18}O and D isotopes

Loryelle Sessegolo¹, Aurélie Verney-Carron¹, Nathalie Valle², Patrick Ausset¹, Sathya Narayanasami³
Sophie Nowak⁴, Chloé Fourdrin⁵, Mandana Saheb¹, Anne Chabas¹

¹LISA, UMR 7583 CNRS / Université Paris Est Créteil / Université Paris Diderot, Institut Pierre Simon Laplace, 61, av du Général de Gaulle, 94010 Créteil Cedex, France

²Luxembourg Institute of Science and Technology, Material Research and Technology Department, Advanced Characterization Platform, 41 rue du Brill, 4422 Belvaux, Luxembourg.

³CEA, DEN, DES, ISEC, SEVT/LCLT, Marcoule, BP17171, 30207 Bagnols sur Cèze cedex, France

⁴Plateforme Rayons X, UFR de Chimie, Université Paris Diderot, Paris, France

⁵Université Paris-Est, Laboratoire Géomatériaux et Environnement, (EA 4508), UPEM, 77454 Marne-la-Vallée, France

* Corresponding author now at: CEA, DEN, DES, ISEC, SEVT/LCLT, Marcoule, BP17171, 30207 Bagnols sur Cèze cedex, France
E-mail address: loryelle.sessegolo@cea.fr

Abstract

Only a few studies deal with the alteration of glass by water vapor. This study aims to investigate the mechanisms and to determine the kinetics of alteration of potash-lime silicate glass typical of the Middle Ages. For that, model glass samples were exposed to different conditions (relative humidity -RH-, temperatures) for several durations. The water vapor used in experiments was enriched in deuterium (D) and oxygen-18 (^{18}O). Results show that mechanisms are highly temperature-dependent. At 50°C, the alteration is driven by interdiffusion, whereas at 20°C, the alteration is mainly governed by hydration without significant ion exchange. Then, the isotopic profiles of H, D, ^{18}O and ^{16}O show that after sorption of water molecules at the glass surface, the diffusing species in the glass matrix are mainly H^+ or D^+ . Concerning the hydration kinetics, they evolve exponentially with time in the first stages of the alteration. Moreover, at 50°C, the hydration follows a linear trend below 83% RH and strongly increases for higher RH values.

Keywords: glass alteration; atmosphere; Secondary Ion Mass Spectrometry; isotopic tracing; mechanisms; kinetics

1) Introduction

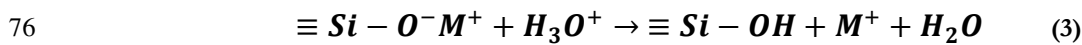
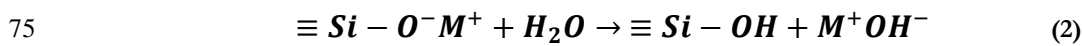
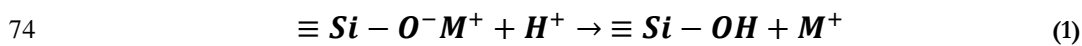
Many stained glass windows constituting the religious heritage were elaborated during the medieval period. At this time, they were composed of a low silica content (~50 wt.%) and a high potassium and calcium content (~15-20 wt.% for each oxide). Because of this composition, medieval glasses are less durable than modern glasses [1], [2]. On buildings, they have been altered by different physicochemical processes caused by atmospheric factors during several centuries. Weathering has been observed for a long time. Indeed, in 1563, B. Palissy already mentioned that the alteration of glasses can be due to the action of the rain [3].

42 The complexity of the atmosphere lies in its multiphase nature (water-unsaturated and liquid
 43 phases), in its content (gases and particles) and its changing nature (daily, weekly and seasonal
 44 cycles). The alteration degree of stained glass windows depends on the climate and local exposure
 45 conditions. On buildings, glasses may be subjected to conditions sheltered from rainfalls, or not.
 46 In the first case, water vapor is the only water supply on the glass surface and thus the key factor
 47 of the alteration. In the second case, glasses are also subject to episodic rainfalls. In Paris (France)
 48 for example, ~6% of cumulative time corresponds to rain (MétéoFrance data: 548 h/year on
 49 average between 1961 and 1990 in Paris). Therefore, the glass is essentially exposed to gaseous
 50 water and its amount can be measured with the relative humidity parameter (RH). This factor is
 51 expressed in % and corresponds to the P/P_0 ratio with P the partial pressure of water vapor in
 52 the air at a temperature T and P_0 the equilibrium vapor pressure at the same temperature.
 53 However, the alteration in vapor phase is often considered as negligible.

54 Relative humidity and the nature of glass affect the number of water molecules adsorbed on the
 55 surface of the material [4]. Asay and Kim, 2005 [5] studied this adsorption on the surface of a
 56 silicon oxide using the Fourier Transform InfraRed (FTIR) spectroscopy - Attenuated Total
 57 Reflectance technique. They showed that between 0 and 30% RH, a "icelike" structure is formed
 58 by the accumulation of several layers of water molecules (up to three). Between 30 and 60% RH,
 59 only one additional layer adsorbs and has a transition structure, whereas above 60% RH, water
 60 molecules accumulate over the first layers but have a structure of liquid water. Near 100% RH,
 61 the water condenses and passes to the liquid state.

62 Few studies evaluated the effect of water vapor on glass. Existing studies have been performed
 63 mainly on nuclear glasses at high temperatures and high RH [6][12]. However, they all
 64 demonstrated the important impact of vapor-induced alteration.

65 Water vapor leads to the same alteration mechanisms than in water-saturated medium: hydration,
 66 interdiffusion, dissolution and precipitation of secondary phases. The hydrolysis of the silicate
 67 network can sometimes take the form of pitting. Nevertheless, it seems that interdiffusion is the
 68 main mechanism [6], [7]. This process is also known as leaching or selective/non-stoichiometric
 69 dissolution. It corresponds to the exchange between hydrogenated species from the environment
 70 and modifier cations from the glass [13]–[15]. Because of the species migration, the glass surface
 71 is hydrated and modifiers cations are released into the medium, inducing modifier depletion at
 72 the glass surface. Interdiffusion can be expressed according to the intervening hydrogen species
 73 (H^+ , H_2O , H_3O^+) in the following three forms:

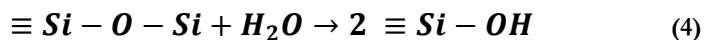


77 With M a modifier cation.

78 It should be noted that the hydration of glass can sometimes occur without ion exchange. It was
 79 mainly observed in atmosphere [6], [7], [16], [17]. In this case, the hydrated layer is not depleted in
 80 alkalis and alkaline-earth elements as they remain in the altered layer.

81 Dissolution, or hydrolysis of the vitreous network, corresponds to the action of water on the
 82 glass network, breaking the Si-O-Si bonds (and some other as Si-O-Al). The chemical reaction
 83 can be described as follows:

84



85 From these mechanisms, different phases can be formed. The main part of the alteration layer
 86 called gel consists of amorphous silica and other few soluble elements such as aluminum or iron.
 87 This layer is supposed to be formed by *in situ* silanol hydrolysis / condensation reactions in the
 88 hydrated glass (e.g. [21]–[23] on nuclear glasses and [24], [25] on medieval glasses) or by an
 89 interfacial coupled dissolution – precipitation process as a function of the conditions (pH, glass
 90 composition, etc.) [26], [27]. Secondary phases are composed of exogenous elements and species
 91 from the glass. For stained glass windows, the exogenous elements are mainly air pollutants: CO₂,
 92 SO₂ and NO_x [28]–[32]. They can be brought in gaseous form or be dissolved in rainfalls. In
 93 addition, particles may be deposited on the surface of glasses (soot, marine aerosols, mineral dust
 94 or metallic particles). These species can react with modifier cations (K⁺, Ca²⁺, Mg²⁺, Na⁺) released
 95 from the glass [1], [33], [34] and form crystallized salts on the surface or inside cracks, mainly
 96 carbonates (calcite) and sulfates (syngenite, gypsum) [1], [33]–[36].

97 Interdiffusion and dissolution rates under water-unsaturated conditions depend on two main
 98 factors: temperature and RH. Moreover, the gaseous content of the atmosphere can also impose
 99 rather acidic or basic conditions on the glass surface [37]. The alteration rates are generally lower
 100 than with liquid water [7]. Neeway et al., 2012 [12], based on experiments at 100 %RH and at very
 101 high surface/volume ratio in saturated condition, demonstrated that it is not possible to compare
 102 the alteration induced by liquid and gaseous water. The comparison of the alteration states of
 103 ancient stained glass windows from the XIVth c. exposed to atmosphere and buried in soil shows
 104 very different alteration thicknesses. Thickness of alteration layers are between 50 and 220 μm in
 105 atmosphere and up to 1.3 mm for buried samples [32]. The average alteration rates vary therefore
 106 from 0.1 to 0.3 μm/year for samples in the atmosphere and from 0.8 to 1.6 μm/year for buried
 107 medieval glasses.

108 However, there are some cases where higher alteration rates in unsaturated conditions have been
 109 reported (Alloteau et al., 2017 [16] for a mixed alkali lime glass and Neeway et al., 2012 [12] for a
 110 nuclear glass). Moreover, the alteration rate measured for a glass exposed to liquid water after a
 111 previous high RH exposure may be greater than the alteration rate of a glass only subjected to
 112 liquid water (without prior exposure to RH) [7], [12]. This can be explained by the retention of
 113 mobile species (modifiers) in the altered layer likely to be leached in contact with H₂O₀. This
 114 could be expected for stained glass windows subject to alternation between water-saturated (rain)
 115 and unsaturated phases (RH).

116 The mechanical and kinetic studies available in literature concern mainly nuclear, obsidian or
 117 soda-lime-silica glasses. There is a lack for medieval stained glass windows while they are mostly
 118 subjected to water-unsaturated condition in atmosphere. To gain insights on these particular
 119 conditions, this study aims to investigate the alteration mechanisms and kinetics of a potash-lime
 120 silicate glass in unsaturated medium. The experiments were carried out in simulation chambers at
 121 several temperatures, RH values and durations. The water vapor used was enriched in deuterium
 122 (²H = D) and ¹⁸O in order to track these isotopes within the glass, to determine the mechanisms
 123 and to measure their respective rates. The evolution of the glass surface chemistry was
 124 characterized using Secondary Ion Mass Spectrometry (SIMS). Optical and scanning electron
 125 microscopies (SEM) were used to follow surface morphology changes. Identification of
 126 secondary phases was done using Energy Dispersive Spectroscopy (EDS) coupled to SEM, X-
 127 Ray Diffraction (XRD) and Raman spectroscopy.

128

129 **2) Material and methods**

130 **2.1. Glass**

131 The experiments were carried out on SG3 model glass monoliths. This glass was previously
 132 described in [38]. Briefly, ultrapure silica, oxides and carbonates were molten together for 2 hours
 133 at 1400°C in a platinum crucible placed in an electric oven. The melted glass was then poured
 134 onto a metallic plate and annealed 2 hours at 560°C (with a cooling from 10°C/min up to 460°C
 135 and then a natural cooling) in a graphite crucible. Its composition is typical of medieval Si-K-Ca
 136 glass (Table 1). Monoliths of $2.5 \times 2.5 \times 0.3 \text{ cm}^3$ and polished down to the quarter of microns.

137

	SiO ₂	Al ₂ O ₃	K ₂ O	CaO	MgO	MnO	Na ₂ O	Fe ₂ O ₃	P ₂ O ₅
wt. %	51.3	1.8	19.2	16.8	4.0	1.0	1.1	1.2	3.8

138 Table 1. Average model glass composition (SG3) in wt.% measured using SEM-EDS on 10 areas
 139 on the bulk glass. The uncertainty is $\pm 0.1 \%$ for all elements.

140

141

142 **2.2. Experimental method**

143 Samples were placed in atmospheric simulation chambers with controlled temperature and
 144 relative humidity. The climatic chambers consisted of hermetic boxes with a bottom tank
 145 containing water in which hygroscopic salts were dissolved up to saturation to control the RH
 146 (Table 2) (see also [24]).

147 For experiments carried out at 20°C, the water (containing hygroscopic salts) was composed of a
 148 mixture of 10% H₂¹⁸O₀ and 90% D₂¹⁶O₀ (Eurisotop®). After equilibrium with the atmosphere
 149 of the chamber, the vapor is thus partly composed of D₂¹⁸O. It is to be noted that the isotopic
 150 ratios of D and ¹⁸O in the vapor phase were not measured. ¹⁸O was used in order to track the
 151 apparent diffusion of oxygen in glass (similarly to [23]). The presence of D in glass reflects its
 152 apparent diffusion during the experiments whereas the presence of H can also be due to the
 153 storage step of samples (ambient contamination) before SIMS measurements even if samples
 154 were stored in desiccator and under vacuum to limit contaminations. At 50°C, D and ¹⁸O were
 155 not used because the renewal of the water for saline solutions was very frequent due to the
 156 important evaporation of the water at this temperature (Table 2). The natural abundances are
 157 99.757 and 0.205% for ¹⁶O and ¹⁸O respectively; and 99.9885 and 0.0115% for H and D,
 158 respectively.

159

	20 ± 0.1 °C				50 ± 0.7 °C			
Salt	K ₂ SO ₄	NaCl	K ₂ CO ₃	CH ₃ COOK	K ₂ SO ₄	KNO ₃	NaCl	MgNO ₃
Solution	(D ₂ ¹⁸ O)	(D ₂ ¹⁶ O)	(D ₂ ¹⁸ O)	(D ₂ ¹⁸ O)	(H ₂ O)	(H ₂ O)	(H ₂ O)	(H ₂ O)
Average RH (%)	91 ± 3	68 ± 2	41 ± 11	29 ± 11	95 ± 3	83 ± 3	76 ± 3	55 ± 9
Time (months)	3, 9 and 15 + 3 and 9 cycles	3 and 9	3 and 9	3 and 9 (cycles)	4	4	4	4

160 Table 2. Summary of exposure conditions. The term “H₂O” corresponds to the conventional
161 water constituted mainly of ¹H and ¹⁶O. Salts are used to control the RH. Two samples were
162 exposed to RH cycles (90/30 %RH) for 3 and 9 months.

163 In the actual atmosphere, RH evolves daily, weekly and seasonally. According to the values
164 measured for four years by Gentaz, 2011 [39] on a Parisian exposure site (at the top of Saint-
165 Eustache Church), the annual average is 70% RH. The average RH are about 83 and 45% in
166 winter and in the summer period, respectively. The annual extrema are 32% RH for the low limit
167 and 97% RH for the high limit. Therefore, a wide range of RH was chosen, between 30 and 95%.
168 For the temperature, Gentaz, 2011 [39] measured an annual average value of 12°C. Daily
169 averages range from -1 to 25°C, with extreme point temperatures ranging from -8°C to 40°C. As
170 part of our research, two temperature values: 20 and 50°C were selected. The first one was
171 chosen to get closer to realistic conditions and the second one to accelerate processes.

172 Samples were horizontally exposed for 3 and 9 months at 40 %RH, 70 %RH and 90 %RH at
173 20°C (Table 2). One sample was exposed for 15 months at 90 %RH. In addition, two samples
174 were subject to humidification (at 90% RH for 4.5 days) and drying cycles (at 30 % RH for 2.5
175 days) repeated for 3 and 9 months. At 50°C, samples were exposed for 4 months at 55 %RH, 76
176 % RH, 83% RH and 95% RH (Table 2).

177

178 2.3 *Analytical techniques*

179 The upper faces of samples were analyzed using a low vacuum SEM-EDS Hitachi TM3030
180 operating at 15 kV. Samples in cross-section were embedded under vacuum (Jeol JFC-1100E)
181 using an Epofix® resin and polished using SiC paper down to P1200 first and then with diamond
182 powders down to ¼ µm diamond grain. For samples exposed to D₂¹⁸O, the polishing was made
183 using ethanol. Samples were coated with palladium by vacuum evaporation in order to avoid
184 charge effect during SEM observations.

185 X-ray diffraction was conducted on a Panalytical Empyrean diffractometer (45 kV and 40 mA Cu
186 tube, filtered radiation, PIXCel multi-channel detector), in Bragg-Brentano configuration θ - θ . The
187 optics used were a 0.04 rad soller slot, a 10 mm mask, and a 1/16° divergence slot. The specimen
188 holder was a 5-axis cradle (x, y, z, chi, phi) allowing an optimized surface adjustment.
189 Measurements were made between 5° and 90° for all samples, with a pitch between 0.01° and
190 0.03° for a pause time ranging from 300 to 600 s (depending on peak width and intensity).

191 Raman analyses were performed at room temperature using a μ -Raman Renishaw InVia equipped
192 with a Leica DM2700 M microscope. A Nd:YAG laser ($\lambda = 532$ nm, powered at 5 mW) was used
193 as incident monochromatic source. The theoretical spot diameter is 0.7 µm (objective \times 100).
194 Spectra were collected between 30 and 60 times during 1 s each and from 60 to 1840 cm⁻¹.

195 For SIMS analyses, samples were analyzed without any special preparation excepting an ethanol
196 wash and a gold coating. The gold thickness was at least 10 nm. After transport and reception at
197 the Luxembourg Institute of Science and Technology where the SIMS measurements have been
198 carried out, samples were kept under vacuum to avoid any contamination (by H₂O for example).
199 The apparatus used was a CAMECA SC-Ultra type instrument, dedicated to in-depth analysis
200 [40]. Analyses were carried out under Cs⁺ bombardment (4 kV acceleration, 4.5 keV for the

201 impact energy) in two distinct modes: the so-called MCs_x^+ mode ($x = 1$ or 2) and the M^- mode.
 202 For both, M represents the element of interest. The MCs_x^+ mode was used to perform the
 203 elemental analyses (Na, K, Si, P, etc.) while the M^- mode was used for the isotopic measurements
 204 (D/H and $^{18}O/^{16}O$). The primary intensity was adjusted according to the thickness to be
 205 sputtered (between 3 nA and 35 nA). The secondary ions were collected on areas of 60 μm
 206 centered on scanned areas of 200 to 250 μm side. Oxygen isotopic measurements were
 207 performed at high mass resolution ($M/\Delta M = 3000$) to avoid the contribution of isobaric
 208 interferences ($H_2^{16}O$, ^{17}OH , $D^{16}O$) on the isotope 18 of oxygen. The D/H and $^{18}O/^{16}O$
 209 measurements were obtained in two separate analyses. The electron gun was used to compensate
 210 for the charge effects. After analyses, the depth of the analysis craters was measured with a
 211 profilometer (KLA Tencor) to allow the conversion of the sputtering time into depth.

212 2.4. Data processing

213 To evaluate hydration kinetics, the average hydration rate was calculated from the total diffusion
 214 thickness divided by the exposure time.

215 The diffusion coefficient D was also determined. For that, different models can be used to fit the
 216 experimental data. The second Fick's law is commonly used. It admits that, in a unidirectional
 217 space, the flux of the diffusing species is established from the most concentrated medium to the
 218 least concentrated medium. The one-dimensional representation of the diffusion in a semi-
 219 infinite solid is defined for D non-dependent on the depth, such that:

$$220 \quad \frac{\partial C_i}{\partial t} = D \frac{\partial^2 C_i}{\partial x^2} \quad \text{Eq. 1}$$

221 With C_i the concentration of the diffusing species, x the diffusion thickness, t the time, and D the
 222 constant diffusion coefficient.

223 One solution of Eq. (1) expresses the evolution of the concentration C_i as a function of distance
 224 x [41], with D constant, is:

$$225 \quad C_i = C_{i(0)} \operatorname{erfc} \left(\frac{x}{2\sqrt{Dt}} \right) \quad \text{Eq. 2}$$

226 The Fick's model considers only a single diffusion coefficient attributed to a diffusing specie.
 227 Since interdiffusion is an ion exchange between hydrogenated species and modifier ions, it
 228 imposes an interdependence between the diffusion coefficients of these two species involved.
 229 Moreover, the reactivity of the hydrogenated species (adsorption, hydrolysis) may result in their
 230 slower diffusion than that of the modifier cations.

231 Doremus, 1975 [13], introduced a non-constant interdiffusion coefficient (\tilde{D}):

$$232 \quad \tilde{D} = \frac{D_M}{1+b \times C_M} \quad \text{with: } b = \frac{D_M}{D_H} - 1 \quad \text{Eq. 3}$$

233 With D_M the diffusion coefficient of a modifier cation, D_H the diffusion coefficient of a
 234 hydrogenated species and C_M the normalized concentration of the modifier cation.

235 The coefficient \tilde{D} can depend on the depth with a higher rate at the glass/solution interface and
 236 then a gradual decrease. The diffusion coefficients D_M and D_H are independent of concentration
 237 and depth. Several ratios D_M/D_H were considered in the literature according to the glass
 238 composition. They are highly variable: 2600 for an aluminosilicate glass at 50°C [42], 100 for an
 239 obsidian at 20°C [43], 105 for a soda lime glass at 90°C [44] and 1.21 for a nuclear glass at 90°C
 240 [45].

241 The solution expressing the concentration of an element (modifier cations or hydrogenated
 242 species) as a function of depth is [13], [46]:

$$243 \quad C_M = C_{M(0)} \frac{1 - \exp\left(-ax/D_H\right)}{1 - b \exp\left(-ax/D_H\right)} \quad \text{or} \quad C_H = C_{H(0)} \frac{\exp\left(-ax/D_H\right)}{1 + b\left(1 - \exp\left(-ax/D_H\right)\right)} \quad \text{Eq. 4}$$

244 With C_M the concentration of a modifier ion, C_H the concentration of hydrogen, $C_{M(0)}$ the initial
 245 concentration of the modifier cation in the pristine glass, a the dissolution rate of the alteration
 246 layer and x the depth.

247 This equation requires knowing the dissolution rate of the alteration layer, which is not possible
 248 in this study. That is why Eq. 5 was used:

$$249 \quad C_H = C_{H(0)} \frac{\operatorname{erfc}\left(\frac{z}{2\sqrt{Dt}}\right)}{1 + b\left(1 - \operatorname{erfc}\left(\frac{z}{2\sqrt{Dt}}\right)\right)} \quad \text{Eq. 5}$$

250 In the following, Fick's model refers to Eq. (2) and Doremus' model to Eq. (5).

251

252 **3) Results**

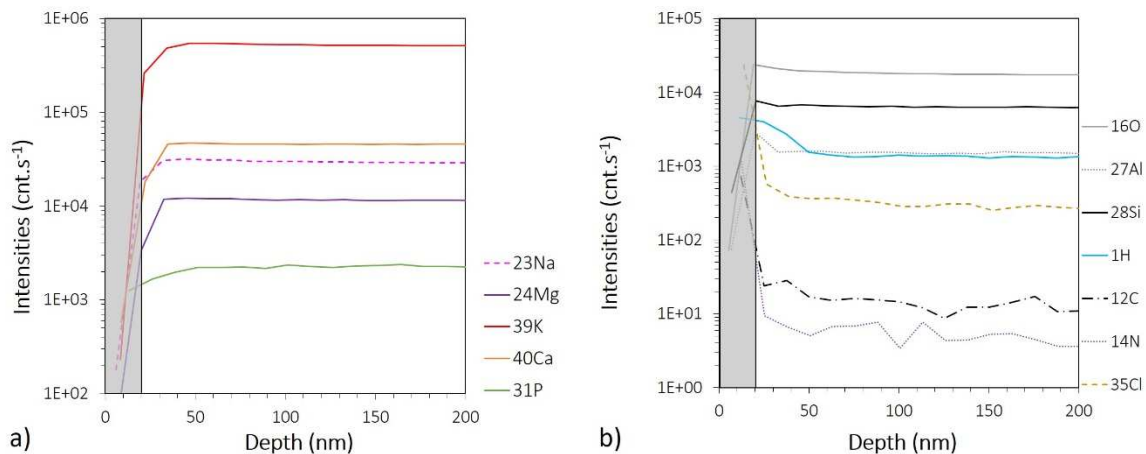
253 Samples will be named in the form "temperature - time - RH". For instance, the sample exposed
 254 for 4 months at 50°C and 95% RH will be referred to as "50-4m95%" in the text.

255

256 **3.1) Glass reference**

257

258



259

260 Fig. 1: SIMS elemental depth profiles of species present in SG3 glass reference (non-altered). The
 261 shaded part corresponds to the metallization of the sample (gold layer). For clarity purpose, the
 262 results were split onto two graphs a) and b).

263

264 The SG3 glass reference analyzed by SIMS indicates that the glass composition over the first 50
 265 nanometers differs from its bulk composition. The first 20 nanometers correspond to the gold
 266 metallization and were not considered. However, K, Ca, Mg, Na (and P to a lesser extent) are
 267 depleted over 15 nm, whereas Si and Al are enriched due to the decrease of previous elements
 268 (Fig. 1a). Hydrogen is enriched on the first 30 nm (Fig. 1b). We can also note the presence of C,
 269 N and Cl, potentially provided by the atmosphere. These analyses thus reveal that the glass,
 270 during its production or its storage, has undergone a slight modification of its surface with
 271 respect to the composition of the glass core.

272 Since silicon content is observed (Fig. 1) and assumed to be constant within the pristine and
 273 altered glass without significant dissolution, intensities of all the elements analyzed were thus
 274 corrected for the Si signal variation. These corrected intensities were afterward normalized with
 275 respect to the intensity of the element i measured in the core of the glass. The first 20 nm (gold
 276 coating) were also removed.

277

278 **3.2) Altered samples**

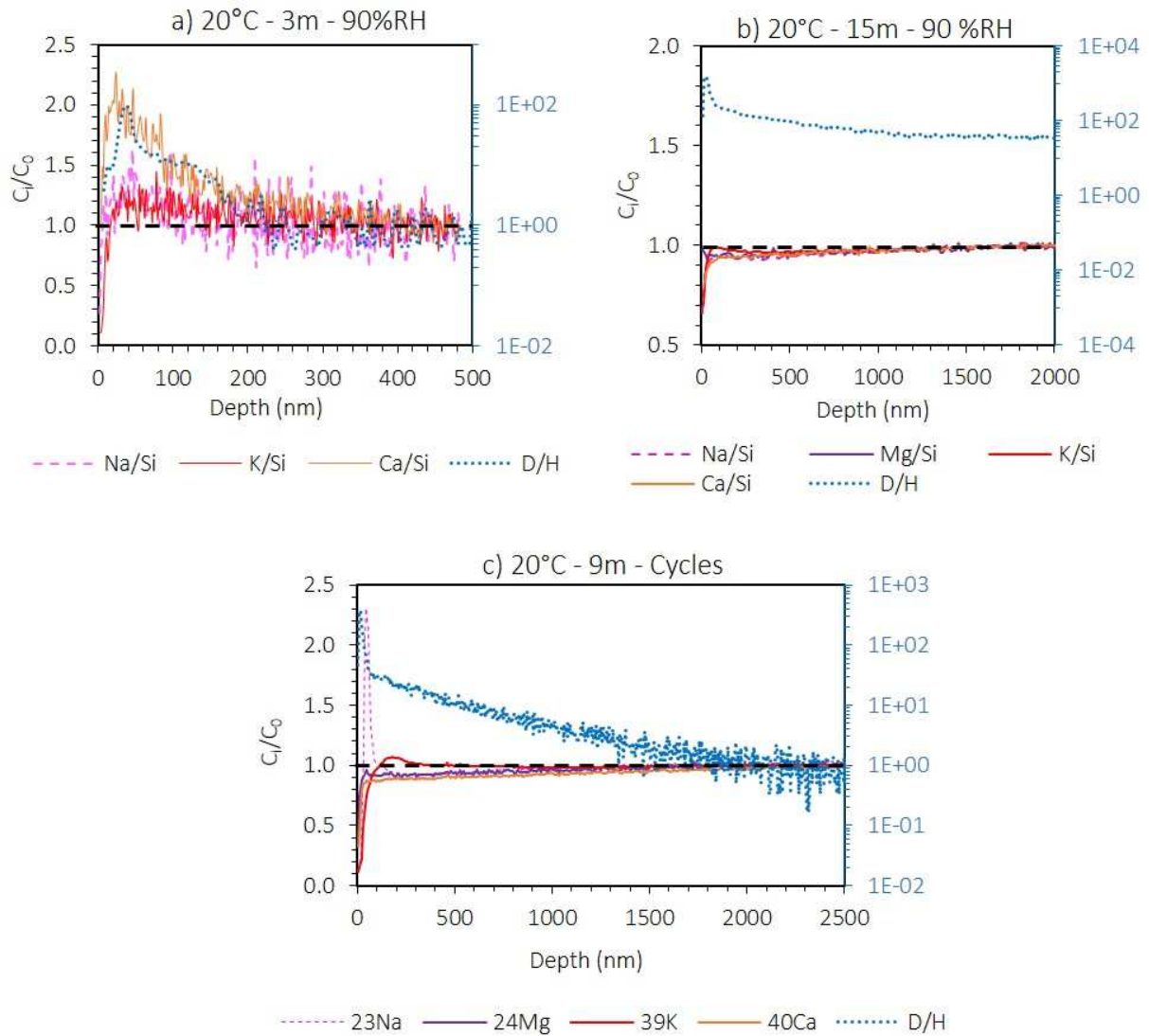
279 The observation of the SIMS elemental profiles after 3 months of exposure at 20°C and 90% RH
 280 (20-3m90%) shows that the modifier cations K, Ca and Na were not leached. They are even
 281 enriched on the first 200 nm, together with the enrichment in D which has diffused in the glass
 282 (Fig. 2a). After 15 months of exposure at the same T and RH (20-15m90%), Ca, Mg K and Na
 283 are very slightly depleted in surface (Fig. 2b). Moreover, this depletion of modifier ions is not
 284 correlated with the diffusion of deuterium that occurs up to 6 μm deep (see the entire D profile
 285 in §3.4)).

286 For the sample placed in 25-90% RH cycles for 9 months at 20°C (20-9mC), a peak of Na is
 287 observed at the surface (Fig. 2c). This could be due to the precipitation of a sodium salt, that is
 288 why this zone was considered to be the external surface. Below this zone, Mg, Ca and Na are
 289 slightly more depleted than the previous sample (Fig. 2c). On the other hand, K does not exhibit

290 depletion and is therefore not leached. This element is even slightly enriched over ~ 100 nm (Fig
291 2c).

292

293



294

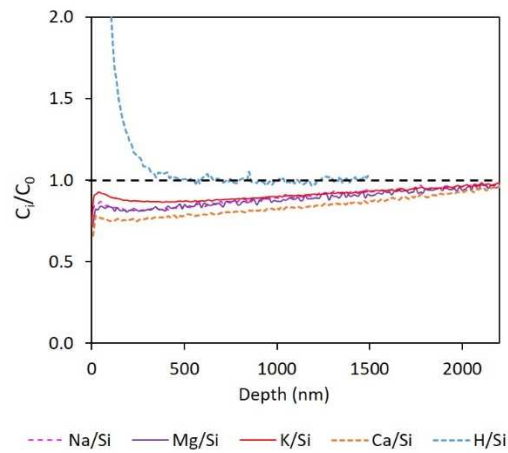
295 Figure 2. Normalized SIMS profiles of a) 20-3m90%, b) 20-15m90% and c) 20-9mC. The
296 horizontal dashed black line is an indication for the eye of normalized pristine content. The blue
297 axis (right axis) refers to the D/H profiles. Mg profiles were not analyzed for 20-3m90%. The
298 D/H profile on graph b) does not reach the value of 1 because the diffusion thickness of this
299 element is $6 \mu\text{m}$ (see Fig. 10 for the entire profile).

300

301 The sample altered for 4 months at 50°C to 55% RH displays depletion of K, Na, Mg and Ca
302 that are much more marked than at 20°C and reach $2 \mu\text{m}$. Conversely, the hydration thickness is
303 only 300 nm (Fig. 3).

304

305



306

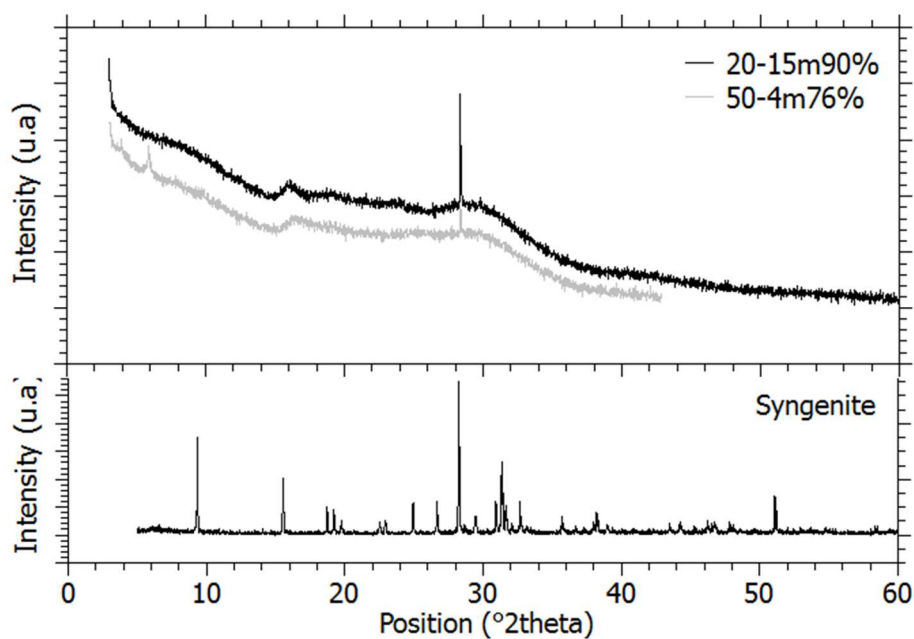
307 Figure 3. Normalized SIMS profiles of the sample 50-4m55%. The horizontal black line at 1.0 is
308 an indication for the eye of normalized pristine glass content.

309

310

311 3.3) Identification of secondary phases

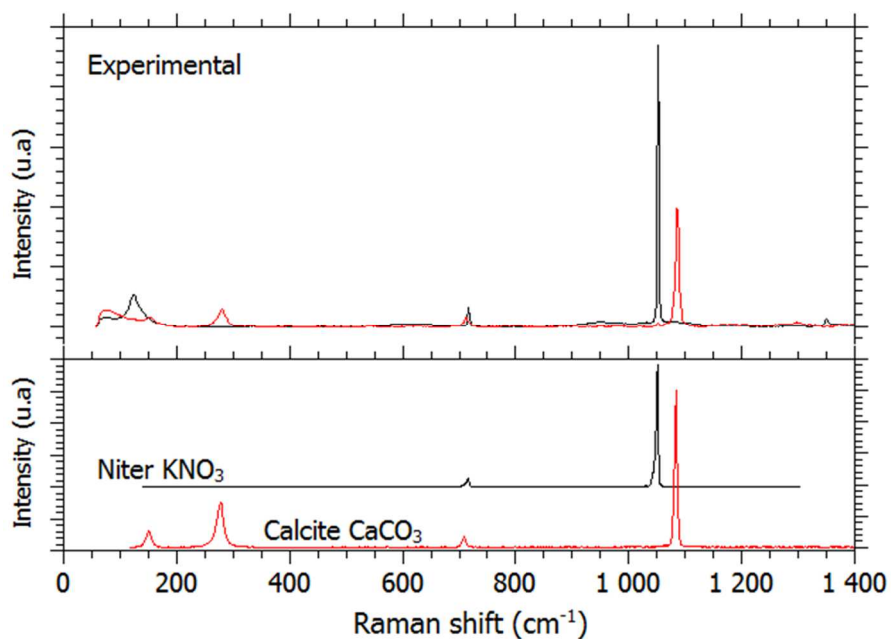
312 At 20°C, very few precipitates were detected on glass surfaces using SEM observation. They were
313 too small to avoid the glass signal overlapping. Moreover, the very low number of crystals does
314 not allow to perform XRD in an effective way. Only syngenite $\text{CaK}_2(\text{SO}_4)\cdot\text{H}_2\text{O}$ could be
315 identified using this technique on 20-15m90% (Fig. 4). Using Raman spectroscopy, few nitrates
316 KNO_3 (niter) and carbonates CaCO_3 have been found (Fig. 5). KNO_3 was detected on 20-
317 9m40% and 20-9m70%. CaCO_3 was found on sample 20-9m90%. It is difficult on Raman
318 spectra to identify if CaCO_3 is calcite, aragonite or vaterite since peaks are very close to each
319 other.



320

321 Figure 4. XRD diffractograms of two samples and comparison with that of syngenite.

322



323

324 Figure 5. Raman spectra of two crystallized phases found on the surface of 20-9m40% and 20-
 325 9m90% (black and red curves, respectively, on the upper graph). Reference spectra of KNO₃ and
 326 CaCO₃ (from RRUFF ID R090001 and R040070) are also presented (lower graph).

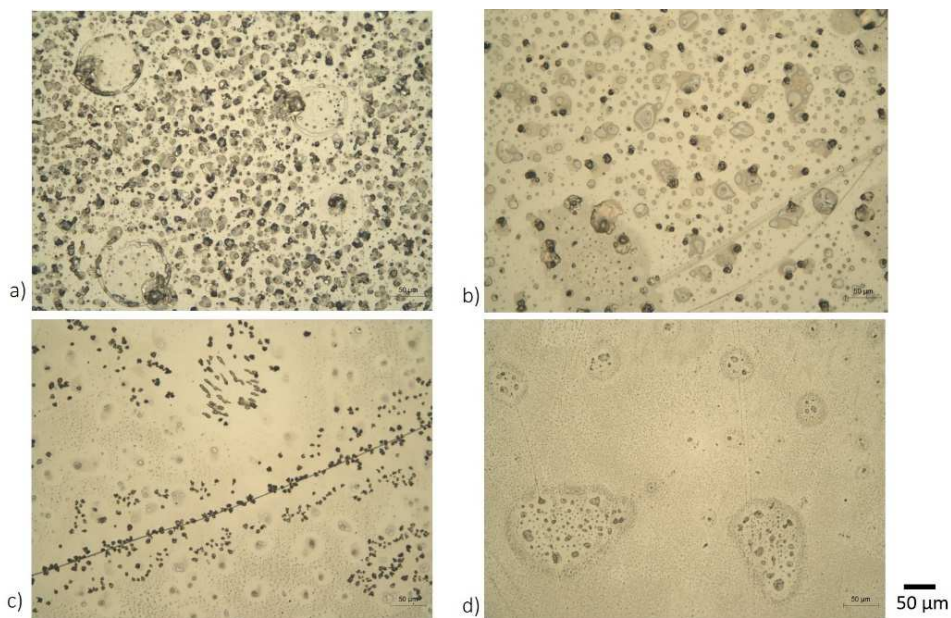
327

328 At 50°C, many secondary phases were formed on glass surfaces. Some of them were formed
 329 during the experiment and are visible to naked eye. Other ones were formed after drying and

330 storage into a desiccator prior to analyses. The precipitation is dependent of the phase solubility
331 and some salts have crystallized when water has evaporated from the surface.

332

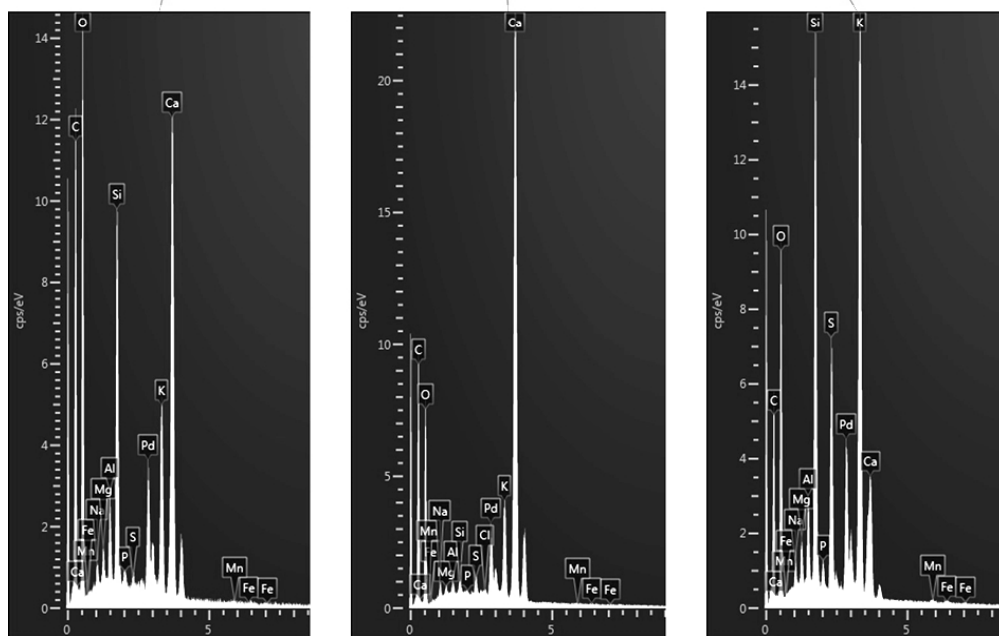
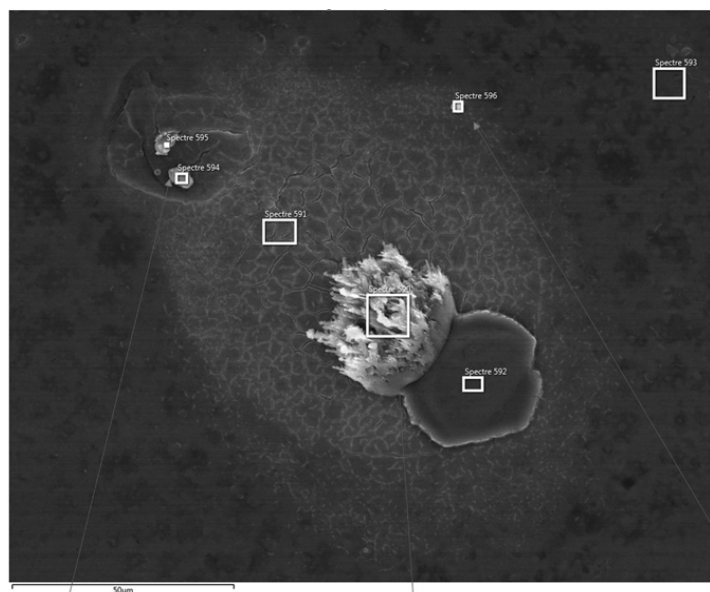
333 With optical microscopy, it is possible to observe that the higher the RH, the higher the quantity
334 of secondary phase precipitation (Fig. 6).



335

336 Figure 6. Optical images of the glass surfaces exposed for 4 months at 50°C at a) 95 %RH, b) 83
337 %RH, c) 76 %RH and d) 55 %RH. Images were taken after drying in desiccator. Samples were
338 not washed.

339



340
 341 Figure 7. SEM image (backscattered electron mode) of secondary phases at the sample surface
 342 exposed at 50°C, 95% RH for 4 months. Three EDS spectra of three crystals are also presented.
 343 The glass surface spectra is presented in the Supplementary Material S1 and more images and
 344 crystals spectra are presented in the Supplementary Material Fig. S2.

345
 346 SEM-EDS analyses indicated that precipitates are composed of C, K, Ca, S and sometimes of N
 347 or Cl (Fig. 7). Some of them do not seem very well crystallized (Fig. 7). Carbon can be found
 348 coupled with K and Ca, suggesting the presence of calcium and potassium carbonates. The
 349 presence of S could be explained by the precipitation of calcium and/or potassium sulfates and
 350 the presence of Cl and N by the formation of halite (NaCl), sylvite (KCl) or potassium nitrate
 351 (KNO₃).

352 XRD analyses confirm the presence of syngenite CaK₂(SO₄)·H₂O on 50-4m76% (Fig. 4).
 353 Moreover, it is possible to observe a small peak located at about 6° (2θ) (or 15 Å) that can be

354 attributed to an aluminosilicate containing Na, Mg and Fe, especially to a phase similar to
355 montmorillonite ([47], [48]).

356 Finally, unfortunately, it was not possible to perform Raman analyses on samples altered at 50°C
357 to precisely identify all the crystalline phases.

358

359 All the phases identified at 20 and 50°C are commonly found on stained glass windows surfaces
360 exposed to the real atmosphere, especially syngenite and Ca-carbonates. A phase such as
361 montmorillonite is rare but some clays were already observed [49], [50]. Salts result generally from
362 the elements coming from the environment (C, N, Cl and S) and alkalis or alkaline-earth elements
363 coming from the glass [49], [51].

364 Contamination by the saline solutions cannot be totally excluded. A hypothesis could be that S, N
365 or Cl are provided by saline solutions and can have migrated to the samples surfaces. Indeed,
366 hygroscopic salts used for some saline solutions were K_2SO_4 , KNO_3 , NaCl and MgNO_3 (Table 2).
367 However, these salts do not explain all precipitations. Indeed, Cl is an element present on all
368 sample surfaces, whatever the chamber, but it was not introduced in salt form inside each saline
369 solution. It can be originated from the tap water used to dissolve salts. However, chlorate salts
370 also are commonly observed on glasses exposed to the real atmosphere [49], [50].

371

372

373 *3.3) Diffusing species*

374

375

376

377

378

379

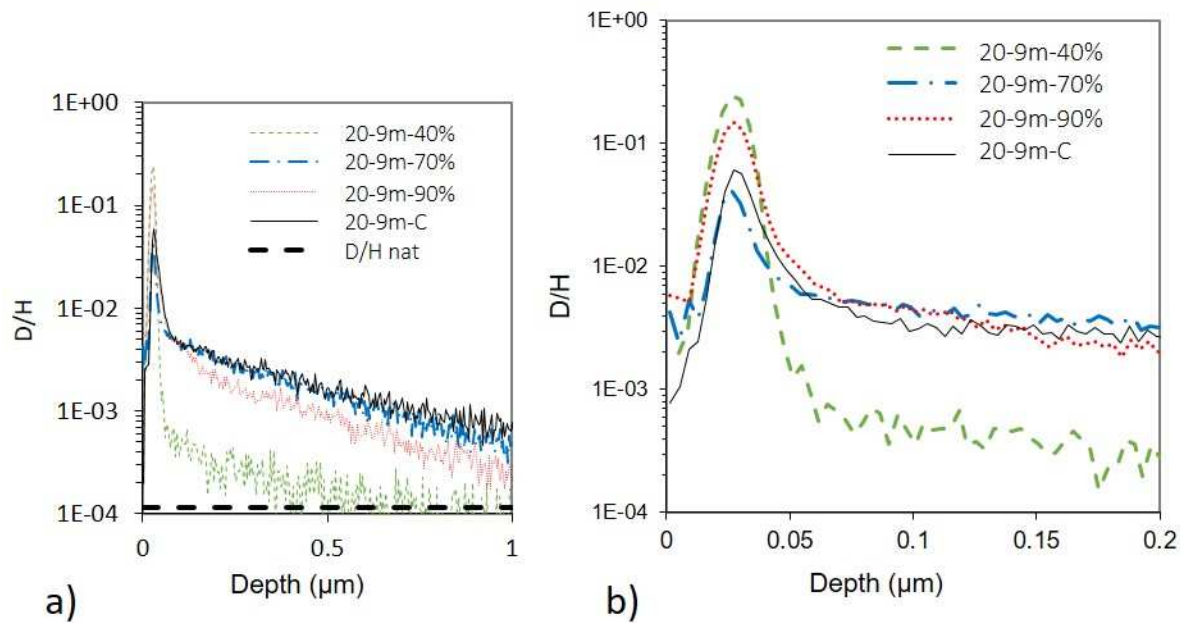
380

381

382

383

384



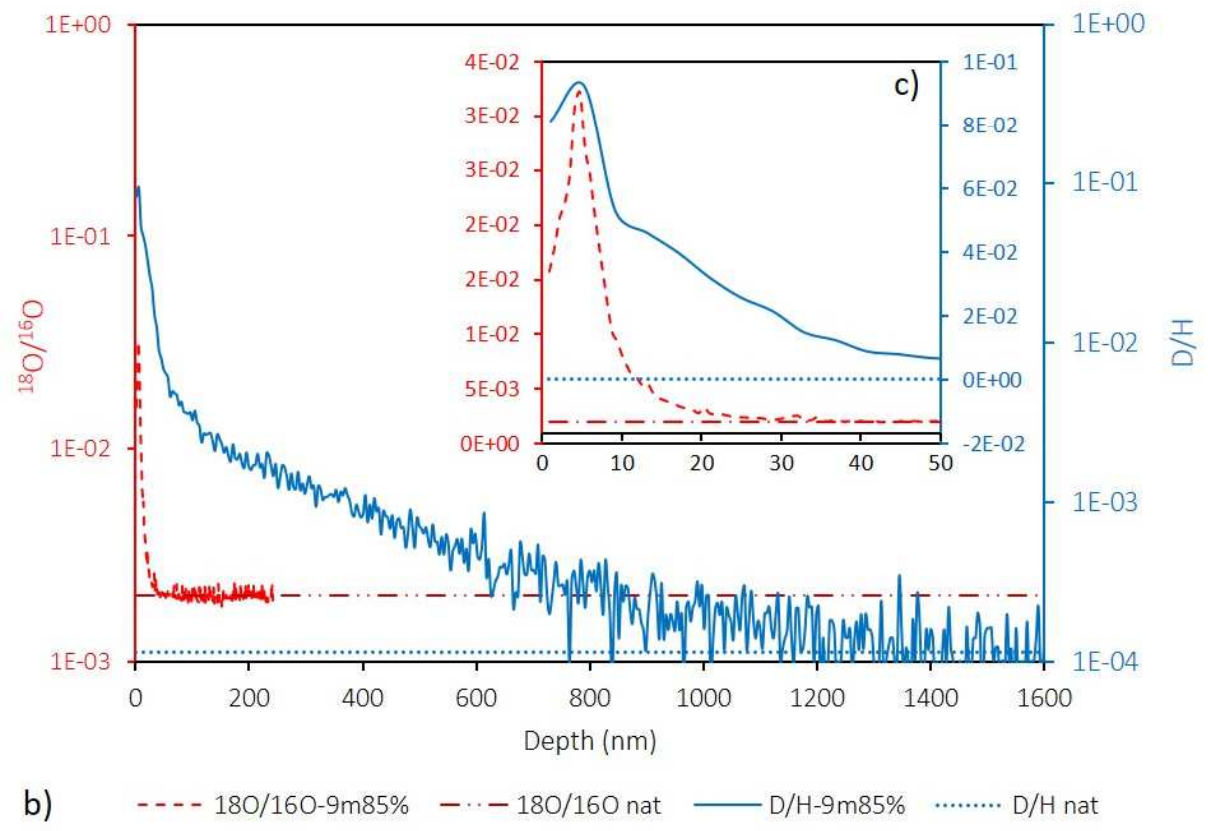
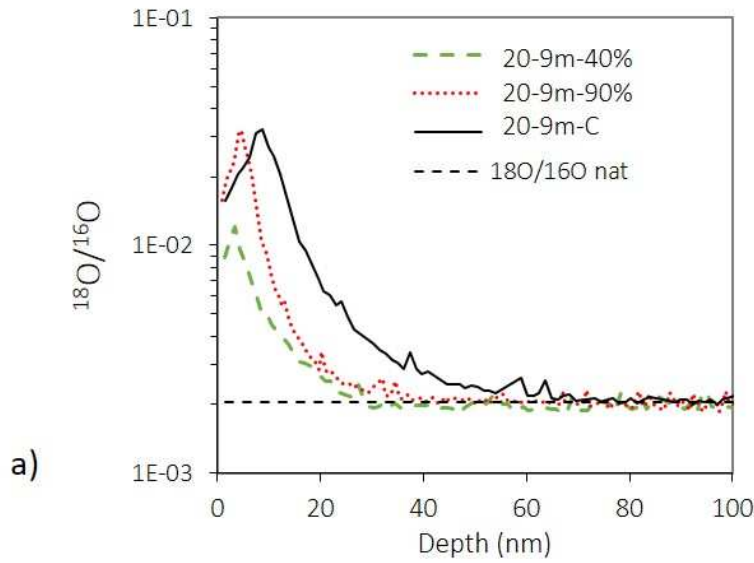
385

386 Figure 8. SIMS profiles of D/H for the samples exposed at 20°C for 9 months at several RH. b)
 387 Zoom of a) to observe the first peaks.

388

389 Figure 8 presents the evolution of D/H on the surfaces of samples exposed at 20°C for 9
 390 months and increasing RH values (20-9m-40%, 20-9m-70%, 20-9m-90%, 20-9m-C). Without
 391 discussing the total thickness of diffusion of D (see §3.4), it is possible to compare the
 392 morphology of D/H profiles. They are all constituted of a first strong peak on surface and then a
 393 decreasing concentration gradient in depth. First strong peaks are located at the same depth and
 394 have a similar width. As their location is independent of the RH, they can be associated with the
 395 adsorption of water molecules.

396



397

398 Figure 9. a) SIMS profiles of $^{18}\text{O}/^{16}\text{O}$ for the samples exposed at 20°C for 9 months at several
 399 RH. b) and c) correspond to the correlation of $^{18}\text{O}/^{16}\text{O}$ and D/H peaks (SIMS profiles) for 20-
 400 9m90%. c) is a window that targets the beginning of the curves. “ $^{18}\text{O}/^{16}\text{O}$ nat” and “D/H nat”
 401 corresponds to the ratio of natural abundances.

402

403 For the diffusion of ^{18}O (Fig. 9a), the shape of profiles is different from that of D. Here, only a
 404 first peak is observable on sample surfaces. ^{18}O does not diffuse in depth in contrast to D (Fig.
 405 9b). Moreover, this peak is pretty well correlated with the D/H strong peak (Fig. 9b and c).

406 Therefore, from these observations, it is possible to point out that: 1) D diffuses without O, thus
 407 on the ion form D⁺ and 2) first peaks can be associated to the adsorption of D₂¹⁸O at the glass
 408 surface.

409

410 **3.4) Hydration thickness**

411 The evolution of the diffusion depth of the hydrogenated species (H or D) as a function of T and
 412 RH can allow the determination of the rate law for glass hydration as a function of these two
 413 parameters.

414 **3.4.1. Evolution as a function of time**

						Fick's Adjustment	Doremus' Adjustment		
T (°C)	Time (months)	RH (%)	Total thickness (µm)	Average rates (µm.year ⁻¹)	half-fall depth (nm)	D _H (m ² .s ⁻¹)	b	D _H (m ² .s ⁻¹)	D _M (m ² .s ⁻¹)
20	9	40	0.40	0.53	13.5	2.5 × 10 ⁻²⁴	-0.95	1.0 × 10 ⁻²⁴	5.0 × 10 ⁻²⁶
20	3	70	0.35	1.40	15.0	9.0 × 10 ⁻²²	0	4.0 × 10 ⁻²²	2.0 × 10 ⁻²²
20	9	70	1.60	2.13	15.2	3.0 × 10 ⁻²¹	1	3.0 × 10 ⁻²¹	6.0 × 10 ⁻²¹
20	3	90	0.20	0.80	14.3	9.0 × 10 ⁻²¹	1	1.5 × 10 ⁻²⁰	3.0 × 10 ⁻²⁰
20	9	90	1.00	1.33	13.5	3.0 × 10 ⁻²¹	5	3.0 × 10 ⁻²¹	1.8 × 10 ⁻²⁰
20	15	90	6.74	5.39	58.3	9.0 × 10 ⁻²⁰	6	9.0 × 10 ⁻²⁰	6.3 × 10 ⁻¹⁹
20	3	cycle	1.00	4.00	267.0	2.5 × 10 ⁻¹⁹	0	2.5 × 10 ⁻¹⁹	2.5 × 10 ⁻¹⁹
20	9	cycle	2.00	2.67	19.5	1.0 × 10 ⁻²⁰	5	1.0 × 10 ⁻²⁰	6.0 × 10 ⁻²⁰
50	4	55	0.16	0.48	22.6	2.0 × 10 ⁻²²	1.4	3.0 × 10 ⁻²²	4.8 × 10 ⁻²²
50	4	76	0.23	0.69	94.2	5.1 × 10 ⁻²²	-0.70	4.0 × 10 ⁻²²	5.0 × 10 ⁻²³
50	4	83	0.28	0.84	33.7	4.0 × 10 ⁻²²	2.2	6.0 × 10 ⁻²²	2.0 × 10 ⁻²¹
50	4	95	1.70	5.10	30.0	1.0 × 10 ⁻²⁰	5	3.0 × 10 ⁻²⁰	1.8 × 10 ⁻¹⁹

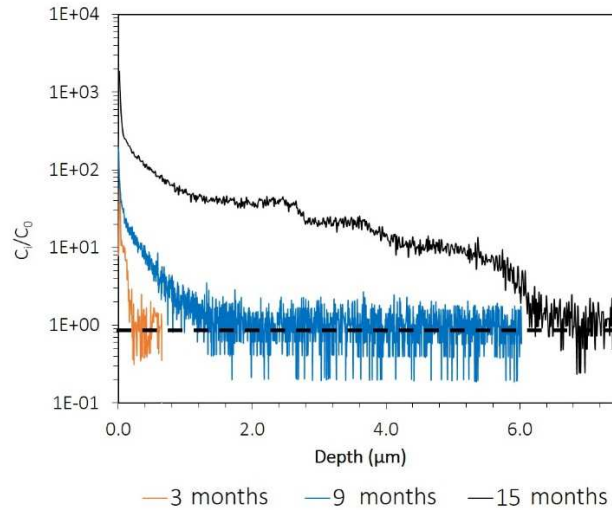
415 Table 3. Total diffusion depth values (in µm), average hydration rates (in µm.year⁻¹), depths at
 416 which the D or H content is halved (half-fall depth, in nm) and diffusion coefficients (in m².s⁻¹)
 417 by fitting with the Fick and Doremus models. D_H corresponds to the diffusion coefficient of H,
 418 D_M to that of a modifier cation and b = (D_M/D_H) - 1.

419

420

421

422 The hydration depth for D increases with exposure time (Fig. 10). Although the literature reports
 423 an evolution of the hydration thickness as a function of t^{1/2} [52], [53], here it evolves exponentially
 424 with values of 0.2 µm for 3 months, 1 µm for 9 months and 6.7 µm for 15 months (all at 90
 425 %RH, Table 3). Samples exposed at 70 %RH also present an increase of the hydration rate over
 426 time. Indeed, the distance traveled for deuterium were 0.3 and 1.6 µm after 3 and 9 months of
 427 exposure, respectively which corresponds to average rates of 1.4 and 2.1 µm.year⁻¹, respectively
 428 (Table 3).



429

430 Figure 10. Normalized SIMS depth profiles of D/H for different exposure times at 90 %RH and
 431 20°C.

432 Finally, the D/H profile for 20-15m90% displays a feature that is not observed on other samples:
 433 several steps are observable at different depths (Fig. 10). It is possible that they are associated to
 434 weak variations in the D/H ratio inside the internal atmosphere of the chamber. Indeed,
 435 hygroscopic solution for this chamber was renewed a few times during the experiment.

436

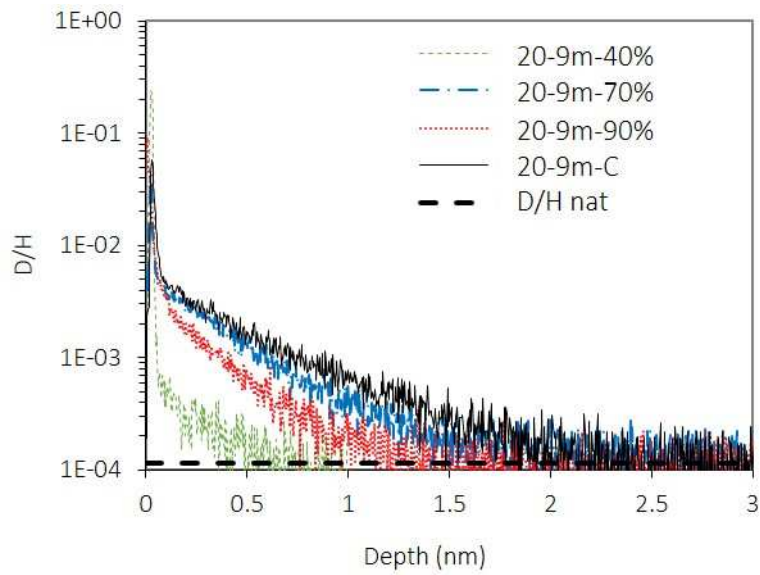
437

438 3.4.2. Evolution as a function of RH

439 For 3 months of exposure, the evolution of the penetration of D is unclear as a function of RH
 440 due to particular events during the experiment or the storage (see Supplementary Material, Fig.
 441 S2).

442 For 9 months of exposure, the penetration of D increases with RH (Fig. 11) except for 20-
 443 9m90% sample presenting 1 μm of D diffusion which is lower than the sample exposed to 70
 444 %RH. This can be due to an experimental bias during the experiment, notably the fact that the
 445 hermetic chamber was open several times in order to make the RH alternation for samples in
 446 cycle conditions. The D diffusion thickness is 0.4 μm and 1.6 μm for 20-9m40% and 20-9m70%
 447 respectively (Fig. 11, Table 3). The sample subjected to low/high RH cycles presents the highest
 448 diffusion depth with about 2.0 μm (Fig. 11).

449



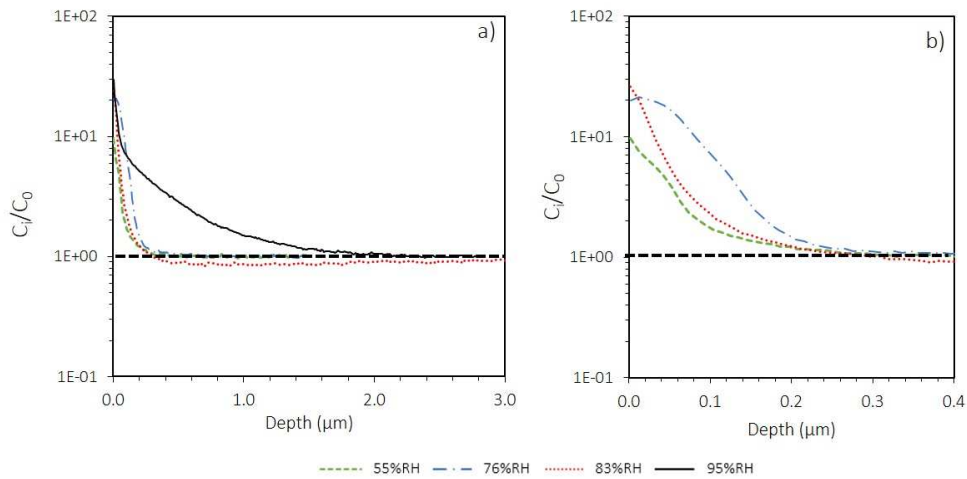
450

451 Figure 11. Evolution of D/H SIMS depth profiles in the glass as a function of RH for samples
 452 exposed for 9 months at 20°C. “D/H nat” corresponds to the ratio of natural abundances.

453

454 At 50°C, samples were exposed for 4 months to H₂O vapor and not D₂¹⁸O because of the very
 455 high evaporation rate. Figure 12 shows that the apparent diffusion distance of H is significant at
 456 95% RH (1.7 μm, Table 3). However, the H penetration is weak and relatively similar for the
 457 three other RH exposures (around 250 nm).

458



459

460 Figure 12. (a) Normalized SIMS depth profiles of H/Si samples exposed at 50°C for 4 months at
 461 different RH. (b) is a window of the beginning of the curves in (a).

462

463

464 **4) Discussion**

465 Table 4 summarizes the results of the literature on different glass composition by providing
466 information on the alteration mechanism, the diffusing species and the activation energy
467 measured over a range of temperatures studied [7], [9], [16], [53]–[58].

468

469

470

471

472

473

474

475

476

477

478

479

480

481

	This study	Anovitz et al., 2008 [54]	Kudriavtsev et al., 2017 [56]	Alloteau et al., 2017 [16]	Cummings et al., 1998[53]; Fearn et al., 2006[58]	Neeway, 2011[57]	Bouakkaz et al., 2018[9]	Abrajano et al., 1989[7]	Kudriavtsev et al., 2018[55]
Glass type	medieval Si-K-Ca	obsidian	obsidian	Si-K-Na	soda glass	nuclear SON68	nuclear SON68	nuclear SRL 131 and PNL 76-68	commercial borosilicate
Composition wt. %	51 % SiO ₂ 19 % K ₂ O 17 % CaO	-	77 % SiO ₂ 10 % Al ₂ O ₃ 5 % K ₂ O	71 % SiO ₂ 11 % Na ₂ O 11 % K ₂ O	73 % SiO ₂ 18 % Na ₂ O 3 % CaO	46 % SiO ₂ 14 % B ₂ O ₃ 10% Na ₂ O	46 % SiO ₂ 14 % B ₂ O ₃ 10% Na ₂ O	44 / 41 % SiO ₂ 14 / 9 % Fe ₂ O ₃ 14 / 10 % Na ₂ O	81 % SiO ₂ 13 % B ₂ O ₃ 4 % Na ₂ O
Mechanism	hydration and interdiffusion	hydration	hydration	hydration	interdiffusion	-	interdiffusion	hydration and interdiffusion (function of the glass)	hydration
Diffusing species	H ⁺ for hydration. Species not defined for interdiffusion	-	H ⁺	H ₂ O	H ⁺ and H ₂ O	-	H ₂ O	H ₂ O	H ⁺
T range	20 and 50°C	n.d	90 to 200°C	80°C	25 to 90°C	125 to 200°C	35 to 125°C	75 to 240°C	90 to 210°C
Ea	Non-arrhenian ?	34.16 Acc. to D	77.6 (H ⁺) 56.7 (¹⁸ O) Acc. to D	non arrhenian	-	43-47 Acc. to v	34.0 Acc. to v 68.0 Acc. to D	137.3 at 95 %HR 74.9 at 100 %HR Acc. to v	90.0 for H ⁺ 80.2 for ¹⁸ O Acc. to D

Table 4. Summary of the results of several studies on the alteration of glasses in unsaturated medium. The mechanism responsible for the alteration is given as well as the diffusing species, the studied temperature range (in °C) and the activation energy measured in this range (in kJ.mol⁻¹). The latter is indicated according to the method of calculation: "Acc. to v" means according to the alteration rate "Acc. to D" means according to the diffusion coefficient of the hydrogenated species. For the compositions, only the percentages of the major oxides are indicated.

4.1. Mechanism of alteration in unsaturated condition

4.1.1. Hydration or interdiffusion ?

After 3 months of alteration at 20°C, modifier cations are not leached (Fig. 2). There is a mobility of species (K, Na, Ca) that migrate and accumulate on the surface without being released by the glass. Regarding to the sample altered in low/high RH cycles, it seems that the mechanism tends to evolve over time towards interdiffusion, but the leaching of the modifier cations is very weak and late with respect to the diffusion of the hydrogenated species (Fig. 2). In addition, the behavior is not general since the leached species do not follow the same trend for all elements and all samples (K is slightly leached at 20-15m90% but not at 20-9mC). At 50°C, the modifier cations are released by the glass and it is possible to clearly observe an interdiffusion mechanism (Fig. 3). Therefore, it seems that the alteration mechanism depends mainly on the temperature with mainly hydration at low temperature (20°C) and interdiffusion at higher temperature. The hydration mechanism alone has also been observed on obsidian [54], [56], alkali mixed Si-K-Na glass [16] and commercial borosilicate glass [55] (Table 4). Anovitz et al. (1999) [17] explained this by a low potential for mass exchange due to the small amount of water on the glass surface (even in the presence of an aqueous film near 100 %RH). Indeed, in immersed medium, the large volume of water allows the solvation and dilution of the released species. Some studies showed that the alteration of glass in water-unsaturated condition causes very rapid precipitation of secondary phases, temporally earlier than in saturated conditions [59]. This is precisely explained by the very small amount of water on the surface of the glass inducing the fast saturation.

Abrajano et al. (1989) [7] found a hydration mechanism on PNL 76-68 nuclear glass and an interdiffusion mechanism on SLR 131 and 165 nuclear glasses (Table 4). The difference was interpreted by authors as a composition effect between the PNL and SLR glasses because they do not contain the same aluminum content (3.5 and 0.5 wt.% respectively). Interdiffusion has been observed for sodium glasses from Cummings et al. (1998), Fearn et al. (2006) and Kudriavtsev et al. (2017) [53], [56], [58] (Table 4).

Thus, according to the data available in the literature, the mechanism does not seem general and depends largely on the composition of the glass and on the conditions of alteration, as demonstrated in this study. Few studies have been performed to well understand which parameters exactly determine the setting up of one mechanism rather than another, although trends are observable. Indeed, sodium glasses still present Na leaching (based on current data and under the conditions tested, Table 4). Conversely, obsidians, containing a very small portion of modifier ion cations (77% SiO₂, 10% Al₂O₃, 5% K₂O, Table 4) present a hydration mechanism only. It could be envisaged that the modifier cation content will define the mechanism governing the alteration with favored interdiffusion in the case of high concentrations of alkali and alkaline earth metals. However, in this study, SG3 glass containing a high level of modifier cations (Table 1), has mechanisms depending on the conditions, notably on the temperature, therefore the modifier content is not the only involved parameter.

Narayanasamy et al. (2019) [47] and Rodrigues et al. (2018) have observed modifier ion enrichments (Na and Ca, respectively) at the glass surface, independently of crystalline phases. In our study, although the samples have never been in contact with the saline solutions, we can wonder about the migration of species from the solution to the internal atmosphere of the chamber. Considering the chamber at 90 %RH in which the over-saturated saline solution was composed of K₂SO₄, if the atmosphere contains a high potassium content in equilibrium with the saline solution, it is possible to imagine an equilibrium at the surface of the glass, or a gradient where the potassium is no longer leached but potentially brought into the glass from the

atmosphere. Observation of the profiles showed that after 3 months of experience in this chamber, K was enriched on the surface (Fig. 2a). After 9 months in cycles 90-25 %RH, K was also enriched. Finally, after 15 months in this chamber, K had not undergone any changes compared to the bulk (Fig. 2c). Therefore, it could be consistent that the presence of a high potassium content in the environment inhibits its departure from the glass [60]. However, this theory is not totally consistent with the fact that Ca and Na are also enriched on the surface of the glass after 3 months of experience, while the environment (and the salts) did not contain these species.

In any case, these enrichments demonstrate the mobility of species on the glass surface despite the absence of leaching. This behavior is important in case of exposure to the real atmospheric environment with the alternation between unsaturated condition and rainfall events. Indeed, Alloteau et al. (2017), Bouakkaz et al. (2018) and Neeway et al. (2012) [9], [12], [16] demonstrated that the alteration in immersed medium is greater if the glass has been previously exposed to water vapor. The authors interpreted this result by the massive leaching of mobile elements that were trapped in alteration products during exposure to water vapor. The enrichment of the modifier cations on the hydration thickness can therefore lead to the same type of behavior in case of future exposure to a rainfall event. As a result, vapor phase alteration can initiate a strong alteration during rainfall events.

4.1.2. Identification of the diffusing species

Whether the alteration mechanism is hydration or interdiffusion, the species involved in these processes are still poorly identified in the literature. Several studies have calculated the H/Na ratios in the leached layer for sodium glasses. By replacing M with Na^+ in the chemical equation (1), H/Na ratio during the exchange must be equal to 1. For equation (2), the ratio must be equal to 2 and for (3) equal to 3. Lanford et al., 1979 [14] determined a H/Na ratio of 2.9 ± 0.3 corresponding to an exchange with H_3O^+ . Houser, et al., 1980 [61] found a ratio of 1.75 and advanced a mixed H^+ and H_2O exchange mechanism. On a nuclear glass (SON68), Ferrand et al. 2006 [62] obtained a ratio of 2.6 ± 0.3 for the ratio $\text{H}/(\text{Na}+\text{Cs}+\text{Li})$ and suggested that the three hydrogenated species have a role in the diffusion. Finally, Dran et al. 1988 [63] who observed a ratio evolving as a function of the depth of the leached layer, also assumed that the three processes (Eq. 1, 2 and 3) can occur and that it depends on the depth.

Cummings et al. (1998)[53] highlighted, on sodium glasses, an equimolar exchange of Na and H at low relative humidity, but 2.8 times more H than Na at high relative humidity, interpreting this result by diffusion of H_2O in addition to H^+ . Fearn et al. (2006) [58] drew the same conclusion from a mixed diffusion of H^+ and H_2O . Alloteau et al. (2017), Abrajano et al. (1989) and Bouakkaz et al. (2018)[7], [9], [16] proposed the unique diffusion of H_2O based notably on the equivalent solubility of D_2O and H_2O and on the equally equivalent diffusion of D and H. Anovitz et al. (2008)[54] also demonstrated a similar diffusion for both water molecules (classical or doped) but did not really discriminate the diffusing species.

Observations in this study suggest that the lack of correlation on depth between the diffusion profiles of ^{18}O and H (or D) rather raises the ionic diffusion of H^+ (and D^+). The presence of a peak of ^{18}O at the extreme surface of the glass linked to a first peak of D highlights the presence of the molecule D_2^{18}O adsorbed (since D peak is not a function of RH). It is to note that if the quantity of water normally depends on the RH, here analyses were conducted inside the vacuum of the machine, therefore the major part of water molecules adsorbed were removed, leaving only

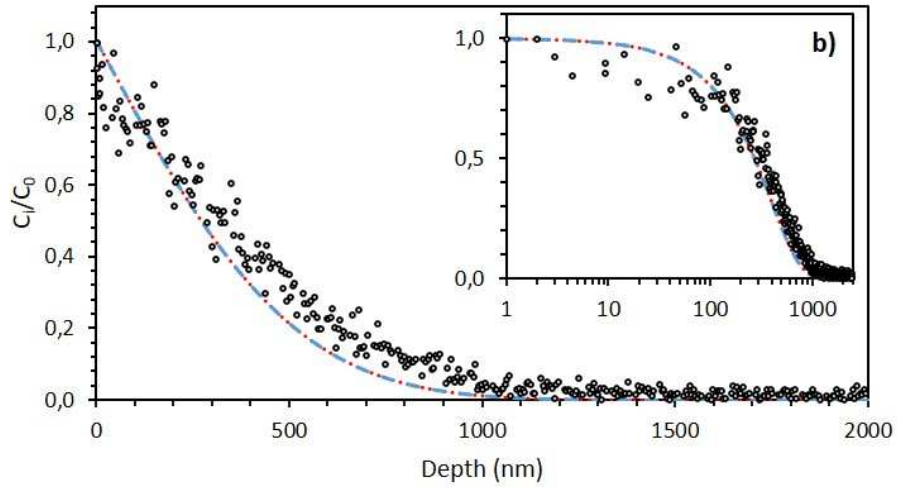
a last layer of molecules [64]. After the adsorbed layer, the diffusion of the protons is observed more in depth, with the absence of ^{18}O (Fig. 8). Kudriavtsev et al. (2018) [55] who carried out aging experiments on borosilicate glasses using oxygen 18, observed some similar results. ToF-SIMS (Time-of-flight-SIMS) profiles have shown an absence of correlation between the diffusion of H and ^{18}O in depth. The authors then interpreted the profiles by a step of dissociation of the H_2O molecules on the surface of the glass and then an independent diffusion of H^+ and ^{18}O in the glass. Results in this study are also in agreement with previous results [24]. The same experiment was performed on ancient stained glass windows dating from the XIVth, with already formed thick alteration layers before the experiment ($\sim 100\ \mu\text{m}$). High-resolution nanoSIMS imaging was used to map the distribution of isotopes at the alteration front on alteration layer cross sections. The results highlighted that hydrogenated species diffuse inside pristine glass without oxygen species.

4.2 Alteration kinetics in unsaturated medium

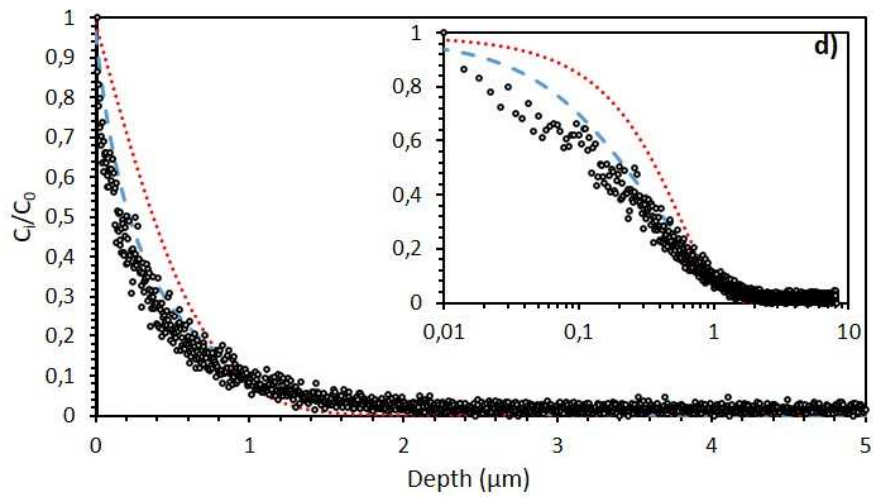
4.2.1. Time dependency and determination of diffusion coefficient

As the hydration thicknesses evolve exponentially with time, it is difficult to determine a diffusion coefficient as it is dependent of the time considered.

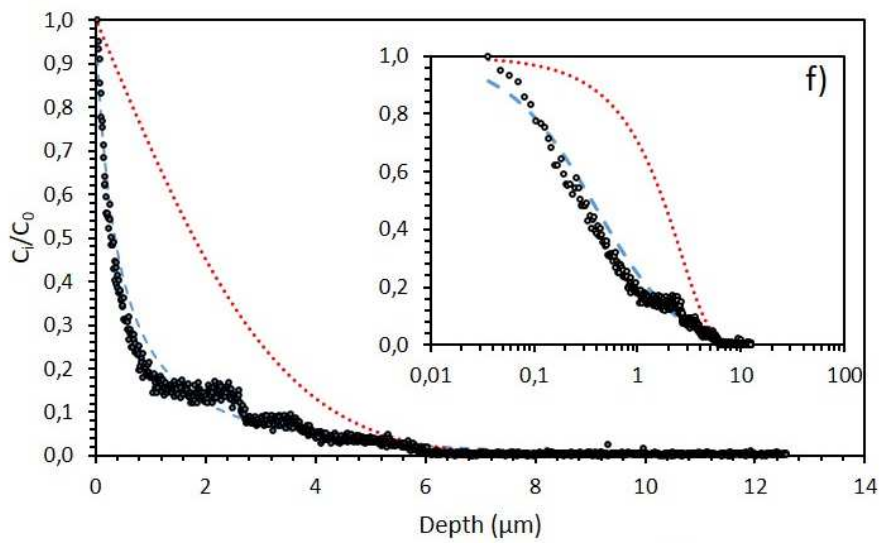
For each experiment, a diffusion coefficient was deduced from Fick's or Doremus' law (see §2.4.). The majority of profiles are not function-type diffusion profile represented by the error function (erf) but they are more complex because of two distinct mechanisms involved: adsorption (intense peak on the surface) and hydration (deep "apparent" diffusion) (Fig. 11). Only the part of the SIMS profiles related to hydration was taken into account to determine H diffusion coefficient with Fick and/or Doremus models (Eq. (2) and Eq. (5)). The fit of curves is presented in Figure 13 and the corresponding diffusion coefficients and adjustment parameters are summarized in Table 3.



a) • Exp Fick - - - Doremus



c) • Exp Fick - - - Doremus



e) • Exp - - - Doremus Fick

Figure 13. Fits of deuterium SIMS diffusion profiles at 20°C with Fick and Doremus models. a, b) 20-3mC, c, d) 20-9mC e, f) 20-15m90%. Little boxes b, d and f) are the same curves in logarithm scale to better observe profiles.

It is possible to observe on Fig. 13 that Fick's model can account for the D penetration depth, but does not allow a good representation of the diffusion profile. This can be observed on others profiles presented in Supplementary Material (Fig. S3). Doremus' model seems to be more consistent to adjust the D/H profiles. According to the literature, the diffusion of the hydrogenated species can be weaker than that of the modifier ions because it is a reactive diffusion (adsorption, hydrolysis). As previously detailed, different authors used b ratios from Doremus' model ranging from 1 to 105 [42], [44], [45]. Here, the best fits with the Doremus' model contain ratios ranging from -0.95 to 6. It was not possible to fit our dataset with only one ratio.

The results confirm that the diffusion coefficient is different for each duration for similar conditions of temperature and RH (Table 3). It can evolve by one order of magnitude between 3 and 9 or 15 months. It seems that a steady state is not reached, which make the comparison with other data concerning other glasses or ancient samples difficult and non-relevant at this stage.

4.2.2. RH dependency

The alteration of the glass depends on the quantity of water available on the glass surface and thus depends on the RH [7], [9], [65]. In this study, the behavior of glasses at 20°C as a function of RH is not very clear. At 50°C, diffusion coefficients at 9 months were plotted on Fig. 14. A RH threshold is observable below which the hydration of glasses little depends on this factor. From 75-80% RH, an exponential growth of the diffusion thickness is observed.

Other authors observed the same behavior involving a threshold value. On SLR 131 nuclear glass, Abrajano et al. (1989) [7] have a very low hydration rate at 40 and 60% RH and an alterability threshold at about 70% RH where hydration exponentially increases. On obsidian, Mazer et al. (1991) [65] observed a similar hydration rate for 60 and 90% RH followed by an increase between 90 and 100% RH (Fig.14). In contrast, Moriya and Nogami (1980) [66] and Cummings et al. (1998) [53] observed a linear increase of the hydration rate throughout a large RH range (from 5 to 100 %RH).

From the hydration rate (in $\mu\text{m}\cdot\text{h}^{-1/2}$) of the Cummings' paper [53], it is possible to deduce the diffusion coefficients using equation 6, and then to plot the $\log(D) = f(\text{RH})$ (Eq. 7) (Fig.14).

$$v = 2\sqrt{\frac{D}{\pi}} \quad \text{Eq. 6}$$

$$D = D_0 \left(\frac{P}{P_0} \right)^{-n} \leftrightarrow \log D = \log D_0 - n \left(\frac{P}{P_0} \right) \quad \text{Eq. 7}$$

With D the diffusion coefficient, D_0 the initial diffusion constant, n the RH coefficient of dependency, P the partial pressure of water vapor in the air at a temperature T and P_0 the equilibrium vapor pressure at the same temperature.

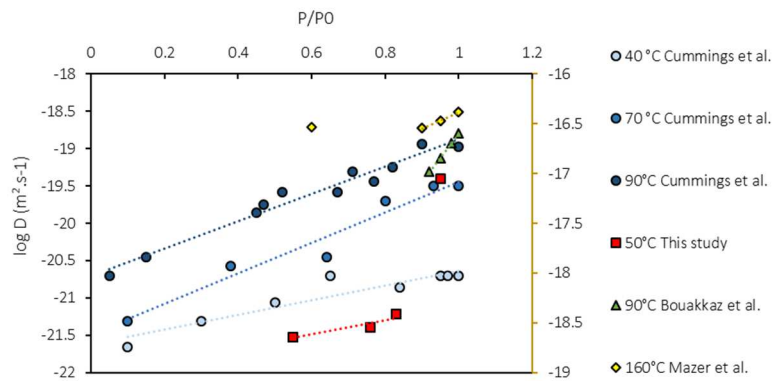


Fig. 14. $\log(D)$ versus P/P_0 : data from Cummings et al. (1998) [53] (light blue to dark blue circles) on sodium glasses, Bouakkaz et al. (2018) [9] (green triangles) on SON68 nuclear glass, Mazer et al. (1991) [65] on obsidian (yellow diamonds associated with the right ordinate), and from this study (red squares) on potash lime glass.

4.2.3. T dependency

Several studies have evaluated the activation energy E_a of glass hydration by water vapor. Values lower than $50 \text{ kJ}\cdot\text{mol}^{-1}$ represent a limiting process corresponding to the species diffusion accumulated at the reaction interface [67], or even to a mixed process coupled with surface reactions [68]. The diffusive limiting process would seem intuitive and adapted to the case of the unsaturated medium since the surface species cannot be evacuated outside the interface. However, the data in the literature are very sparse and authors evaluated E_a between 34.0 and $137.3 \text{ kJ}\cdot\text{mol}^{-1}$ (Table 4). Some authors have determined E_a from the hydration rate and others from the diffusion coefficient. The conversion from one to the other one can be carried out using Equation 5. From the D coefficient, the measured values are $34.2 \text{ kJ}\cdot\text{mol}^{-1}$ by Anovitz et al. (2008)[54] and $68.0 \text{ kJ}\cdot\text{mol}^{-1}$ by Bouakkaz et al. (2018)[9] (Table 4). From the hydration rates, the values measured by Neeway (2011)[57] are between 43 and $47 \text{ kJ}\cdot\text{mol}^{-1}$ (FTIR or ToF-SIMS measurements) and that evaluated by Bouakkaz et al. (2018)[9] is $34.0 \text{ kJ}\cdot\text{mol}^{-1}$. Abrajano et al. (1989)[7] obtained $74.9 \text{ kJ}\cdot\text{mol}^{-1}$ at 100% RH and $137.3 \text{ kJ}\cdot\text{mol}^{-1}$ at 95% RH (Table 4). Kudriavtsev et al. (2018)[55] differentiated the diffusions of H^+ and ^{18}O and calculated two energies of activation from the distinct diffusion coefficients of the two species: $80.2 \text{ kJ}\cdot\text{mol}^{-1}$ (for ^{18}O) and $90.0 \text{ kJ}\cdot\text{mol}^{-1}$ (for H^+) (commercial borosilicate glass, Table 4). On obsidians, these same authors also measured $56.7 \text{ kJ}\cdot\text{mol}^{-1}$ (^{18}O) and $77.6 \text{ kJ}\cdot\text{mol}^{-1}$ (H^+) [56]. Moriya and Nogami (1980)[66] measured values between 75.3 and $83.7 \text{ kJ}\cdot\text{mol}^{-1}$. These very high values seem to represent a process governed by surface reactivity. The experiments were carried out at high RH, which implies a significant amount of available water (or even condensation close to 100% RH). The limiting process based on the diffusion of the dissolved species outside the reaction interface can then evolve into a limiting process of surface reactions.

In the context of this study, it is not possible to verify the Arrhenian behavior of the alteration nor to calculate an activation energy for several reasons as only two temperature points were studied. Moreover, the 70% and 90 %RH data seem to indicate an acceleration of the hydration rate over time. Alloteau (2017)[69] already observed this behavior for mixed alkali Si-K-Na glasses and deduced a non-Arrhenian behavior because of this increasing rate. Finally, the mechanisms are not identical depending on the conditions. By comparing 20-3m70% and 50-4m76% which are the two closest samples in terms of exposure time and RH studied, it is possible to notice that the thickness of diffusion, and thus the hydration rate, are higher at 20°C than at 50°C. Since several authors have shown equivalent diffusion in glass for D₂O and H₂O [54], [70], we hypothesize that it is also identical for H⁺ (diffusing species at 50°C) and D⁺ (diffusing species at 20°C). In addition, the D and H profiles of one sample (20-3m90%) showed similar diffusion for both elements (not shown here). Thus, the lower hydration at 50°C than at 20°C could result from the difference in the mechanism involved in the alteration of the glass with interdiffusion that has a lower rate than for hydration. Indeed, the reactive diffusion can be slower and the process will probably be more thermally activated.

4.2.4. Particular case of sample exposed to low/high RH cycles

The case of samples placed in humidification/drying cycles between 25 and 90 %RH is interesting. Indeed, these samples demonstrate the largest D diffusion thickness (i.e greater than the exposures at a unique RH) for the two durations of exposure tested (3 and 9 months).

At first, mechanical effects due to drying could be considered. The loss of free H₂O molecules in the vitreous matrix during the drying would cause stresses within the network, causing the appearance of microcracks and thus promoting the penetration of new water molecules during a subsequent humidification cycle. However, the hydration mechanism with proton diffusion has been highlighted. Thus, it is possible to assume that there are very few free water molecules in the glass network, which does not satisfy this first hypothesis.

A second hypothesis is the renewal of the water molecules present in the pore network of the gel. The progress of hydration and hydrolysis/condensation (or dissolution/precipitation) in depth can be controlled in part by the porous diffusion of H₂O_(g) molecules in the gel. Thus, during drying of the glass at 25 %RH, most of the water (free and adsorbed) in the pore network is discharged to the internal atmosphere of the climatic chamber. It remains only one monolayer of water adsorbed on the walls of the pores [71]. The following humidification cycle renews water molecules within the gel, available for further alteration.

Conclusion

This study allowed investigating the mechanisms and kinetics of the alteration of stained glass windows under unsaturated conditions. At low temperature, the alteration is mainly governed by a hydration mechanism of the glasses that is not or only very slightly coupled with an ion exchange between the hydrogenated species and the alkaline/alkaline-earth metals. From the uncorrelated isotopic profiles of D and ¹⁸O, it is highlighted that the diffusing species is H⁺ or D⁺. In the hydration process, modifier cations are hydrolyzed but remain in the hydrated glass and seem to be mobile as some enrichments are observed. They can potentially be rapidly released during a rainfall event. Moreover, the 25-90% RH cycle samples present a greater hydration thickness than the other samples subject to a constant RH, demonstrating the importance of the humidification/drying cycles that cause the renewal of the water molecules in

the pore network of the gel, available for further alteration. Regarding the kinetics of hydration, the behavior of the glasses is complex at 20°C compared to 50°C, demonstrating processes undoubtedly strongly thermally activated. This makes the determination of alteration kinetics difficult. However, we could observe an exponential behavior of the hydration rate as a function of the RH at 50°C.

ACKNOWLEDGMENTS

The financial support by the French National Research Agency under the frame of the GLAM project is gratefully acknowledged. The authors wish to thank B. El Adib for supporting the SIMS measurements with in particular the use of contact profilometry.

DATA AVAILABILITY

The raw/processed data required to reproduce these findings can be shared upon request.

REFERENCES

- [1] M. Melcher et M. Schreiner, « Leaching studies on naturally weathered potash-lime-silica glasses », *J. Non-Cryst. Solids*, vol. 352, n° 5, p. 368–379, mai 2006, doi: 10.1016/j.jnoncrysol.2006.01.017.
- [2] G. Woisetschläger, M. Dutz, S. Paul, et M. Schreiner, « Weathering phenomena on naturally weathered potash-lime-silica-glass with medieval composition studied by secondary electron microscopy and energy dispersive microanalysis », *Microchim. Acta*, vol. 135, n° 3, p. 121–130, 2000.
- [3] B. (1510?-1589?) A. du texte Palissy, *Recepte véritable par laquelle tous les hommes de la France pourront apprendre à multiplier et augmenter leurs thrésors*. 1563.
- [4] H. V. Walters et P. B. Adams, « Effects of humidity on the weathering of glass », *J. Non-Cryst. Solids*, vol. 19, p. 183–199, déc. 1975, doi: 10.1016/0022-3093(75)90084-8.
- [5] D. B. Asay et S. H. Kim, « Evolution of the Adsorbed Water Layer Structure on Silicon Oxide at Room Temperature », *J. Phys. Chem. B*, vol. 109, n° 35, p. 16760–16763, sept. 2005, doi: 10.1021/jp053042o.
- [6] A. Abdelouas *et al.*, « A Preliminary Investigation of the ISG Glass Vapor Hydration », *Int. J. Appl. Glass Sci.*, vol. 4, n° 4, p. 307–316, oct. 2013, doi: 10.1111/ijag.12055.
- [7] T. A. Abrajano, J. K. Bates, et J. J. Mazer, « Aqueous corrosion of natural and nuclear waste glasses II. Mechanisms of vapor hydration of nuclear waste glasses », *J. Non-Cryst. Solids*, vol. 108, n° 3, p. 269–288, 1989.
- [8] J. K. Bates, M. G. Seitz, et M. J. Steindler, « The relevance of vapor phase hydration aging to nuclear waste isolation », *Nucl. Chem. Waste Manag.*, vol. 5, n° 1, p. 63–73, 1984.
- [9] R. Bouakkaz, A. Abdelouas, et B. Grambow, « Kinetic study and structural evolution of SON68 nuclear waste glass altered from 35 to 125 °C under unsaturated H₂O and D₂O₁₈ vapour conditions », *Corros. Sci.*, vol. 134, p. 1–16, avr. 2018, doi: 10.1016/j.corsci.2017.12.035.
- [10] W. L. Gong, L. M. Wang, R. C. Ewing, E. Vernaz, J. K. Bates, et W. L. Ebert, « Analytical electron microscopy study of surface layers formed on the French SON68 nuclear waste glass during vapor hydration at 200°C », *J. Nucl. Mater.*, vol. 254, n° 2, p. 249–265, avr. 1998, doi: 10.1016/S0022-3115(97)00349-8.
- [11] A. Jiříčka, J. D. Vienna, P. Hrma, et D. M. Strachan, « The effect of experimental conditions and evaluation techniques on the alteration of low activity glasses by vapor hydration », *J. Non-Cryst. Solids*, vol. 292, n° 1, p. 25–43, 2001.
- [12] J. Neeway *et al.*, « Vapor hydration of SON68 glass from 90°C to 200°C: A kinetic study and corrosion products investigation », *J. Non-Cryst. Solids*, vol. 358, n° 21, p. 2894–2905, oct. 2012, doi: 10.1016/j.jnoncrysol.2012.07.020.
- [13] R. H. Doremus, « Interdiffusion of hydrogen and alkali ions in a glass surface », *J. Non-Cryst. Solids*, vol. 19, p. 137–144, 1975.
- [14] W. A. Lanford, K. Davis, P. Lamarche, T. Laursen, R. Groleau, et R. H. Doremus, « Hydration of soda-lime glass », *J. Non-Cryst. Solids*, vol. 33, n° 2, p. 249–266, 1979.
- [15] A. Y. Wang-hong et R. James Kirkpatrick, « Hydrothermal reaction of albite and a sodium aluminosilicate glass: A solid-state NMR study », *Geochim. Cosmochim. Acta*, vol. 53, n° 4, p. 805–819, avr. 1989, doi: 10.1016/0016-7037(89)90027-6.

- [16] F. Alloteau *et al.*, « New insight into atmospheric alteration of alkali-lime silicate glasses », *Corros. Sci.*, vol. 122, p. 12-25, juill. 2017, doi: 10.1016/j.corsci.2017.03.025.
- [17] L. M. Anovitz, J. M. Elam, L. R. Riciputi, et D. R. Cole, « The Failure of Obsidian Hydration Dating: Sources, Implications, and New Directions », *J. Archaeol. Sci.*, vol. 26, n° 7, p. 735-752, juill. 1999, doi: 10.1006/jasc.1998.0342.
- [18] N. Donzel, S. Gin, F. Augereau, et M. Ramonda, « Study of gel development during SON68 glass alteration using atomic force microscopy. Comparison with two simplified glasses », *J. Nucl. Mater.*, vol. 317, n° 1, p. 83-92, avr. 2003, doi: 10.1016/S0022-3115(02)01705-1.
- [19] S. Gin, I. Ribet, et M. Couillard, « Role and properties of the gel formed during nuclear glass alteration: importance of gel formation conditions », *J. Nucl. Mater.*, vol. 298, n° 1, p. 1-10, sept. 2001, doi: 10.1016/S0022-3115(01)00573-6.
- [20] C. Jégou, S. Gin, et F. Larché, « Alteration kinetics of a simplified nuclear glass in an aqueous medium: effects of solution chemistry and of protective gel properties on diminishing the alteration rate », *J. Nucl. Mater.*, vol. 280, n° 2, p. 216-229, juill. 2000, doi: 10.1016/S0022-3115(00)00039-8.
- [21] S. Gin *et al.*, « The fate of silicon during glass corrosion under alkaline conditions: A mechanistic and kinetic study with the International Simple Glass », *Geochim. Cosmochim. Acta*, vol. 151, p. 68-85, févr. 2015, doi: 10.1016/j.gca.2014.12.009.
- [22] S. Gin, J. V. Ryan, D. K. Schreiber, J. Neeway, et M. Cabié, « Contribution of atom-probe tomography to a better understanding of glass alteration mechanisms: Application to a nuclear glass specimen altered 25 years in a granitic environment », *Chem. Geol.*, vol. 349-350, p. 99-109, juin 2013, doi: 10.1016/j.chemgeo.2013.04.001.
- [23] N. Valle, A. Verney-Carron, J. Sterpenich, G. Libourel, E. Deloule, et P. Jollivet, « Elemental and isotopic (²⁹Si and ¹⁸O) tracing of glass alteration mechanisms », *Geochim. Cosmochim. Acta*, vol. 74, n° 12, p. 3412-3431, juin 2010, doi: 10.1016/j.gca.2010.03.028.
- [24] L. Sessegolo *et al.*, « Long-term weathering rate of stained-glass windows using H and O isotopes », *Npj Mater. Degrad.*, vol. 2, n° 1, p. 17, juin 2018, doi: 10.1038/s41529-018-0038-1.
- [25] A. Verney-Carron *et al.*, « Understanding the mechanisms of Si–K–Ca glass alteration using silicon isotopes », *Geochim. Cosmochim. Acta*, vol. 203, p. 404-421, avr. 2017, doi: 10.1016/j.gca.2017.01.030.
- [26] T. Geisler *et al.*, « The mechanism of borosilicate glass corrosion revisited », *Geochim. Cosmochim. Acta*, vol. 158, p. 112-129, juin 2015, doi: 10.1016/j.gca.2015.02.039.
- [27] R. Hellmann *et al.*, « Nanometre-scale evidence for interfacial dissolution–reprecipitation control of silicate glass corrosion », *Nat. Mater.*, vol. 14, n° 3, p. 307-311, mars 2015, doi: 10.1038/nmat4172.
- [28] V. Kontozova-Deutsch, F. Deutsch, R. Godoi, R. Van Grieken, et K. De Wael, « Urban air pollutants and their micro effects on medieval stained glass windows », *Microchem. J.*, vol. 99, n° 2, p. 508-513, nov. 2011, doi: 10.1016/j.microc.2011.07.003.
- [29] M. Melcher et M. Schreiner, « Leaching studies on naturally weathered potash-lime–silica glasses », *J. Non-Cryst. Solids*, vol. 352, n° 5, p. 368-379, mai 2006, doi: 10.1016/j.jnoncrysol.2006.01.017.
- [30] I. Munier, R.-A. Lefèvre, G.-B. F, et V. M, « Influence of polluted urban atmosphere on the weathering of low durability glasses », *Glass Technol.*, vol. 43, p. 225-237, déc. 2002.
- [31] I. Munier, R.-A. Lefèvre, et R. Losno, « Atmospheric factors influencing the formation of neocrystallisations on low durability glass exposed to urban atmosphere », *Glass Technol.*, vol. 43, p. 114-124, juin 2002.
- [32] J. Sterpenich et G. Libourel, « Using stained glass windows to understand the durability of toxic waste matrices », *Chem. Geol.*, vol. 174, n° 1-3, p. 181-193, avr. 2001, doi: 10.1016/S0009-2541(00)00315-6.
- [33] I. Munier, R.-A. Lefèvre, G.-B. F, et V. M, « Influence of polluted urban atmosphere on the weathering of low durability glasses », *Glass Technol.*, vol. 43, p. 225-237, déc. 2002.
- [34] I. Munier, R.-A. Lefèvre, et R. Losno, « Atmospheric factors influencing the formation of neocrystallisations on low durability glass exposed to urban atmosphere », *Glass Technol.*, vol. 43, p. 114-124, juin 2002.
- [35] L. Gentaz, T. Lombardo, A. Chabas, C. Loisel, D. Neff, et A. Verney-Carron, « Role of secondary phases in the scaling of stained glass windows exposed to rain », *Corros. Sci.*, vol. 109, p. 206-216, avr. 2016, doi: 10.1016/j.corsci.2016.04.005.
- [36] T. Lombardo, C. Loisel, L. Gentaz, A. Chabas, M. Verita, et I. Pallot-Frossard, « Long term assessment of atmospheric decay of stained glass windows », *Corros. Eng. Sci. Technol.*, vol. 45, n° 5, p. 420-424, oct. 2010, doi: 10.1179/147842210X12710800383800.
- [37] A. Ait Chaou, A. Abdelouas, Y. El Mendili, et C. Martin, « The role of pH in the vapor hydration at 175 °C of the French SON68 glass », *Appl. Geochem.*, vol. 76, p. 22-35, janv. 2017, doi: 10.1016/j.apgeochem.2016.11.006.

- [38] L. Sessegolo, A. Verney-Carron, P. Ausset, M. Saheb, et A. Chabas, « Effect of surface roughness on medieval-type glass alteration in aqueous medium », *J. Non-Cryst. Solids*, vol. 505, p. 260-271, févr. 2019, doi: 10.1016/j.jnoncrsol.2018.10.051.
- [39] L. Gentaz, « Simulation et modélisation de l'altération des verres de composition médiévale dans l'atmosphère urbaine », Thèse de doctorat, Laboratoire interuniversitaire des systèmes atmosphériques, Créteil, France, 2011.
- [40] L. Sangely *et al.*, « CHAPTER 15:Secondary Ion Mass Spectrometry », in *Sector Field Mass Spectrometry for Elemental and Isotopic Analysis*, 2014, p. 439-499.
- [41] J. (John) Crank, *The mathematics of diffusion / by J. Crank*. Oxford [England]: Clarendon Press, 1975.
- [42] F. G. K. Baucke, « Investigation of surface layers, formed on glass electrode membranes in aqueous solutions, by means of an ion sputtering method », *J. Non-Cryst. Solids*, vol. 14, n° 1, p. 13-31, janv. 1974, doi: 10.1016/0022-3093(74)90014-3.
- [43] R. R. Lee, D. A. Leich, T. A. Tombrello, J. E. Ericson, et I. Friedman, « Obsidian hydration profile measurements using a nuclear reaction technique », *Nature*, vol. 250, n° 5461, p. 44-47, juill. 1974, doi: 10.1038/250044a0.
- [44] W. A. Lanford, « ¹⁵N hydrogen profiling: Scientific applications », *Nucl. Instrum. Methods*, vol. 149, n° 1, p. 1-8, févr. 1978, doi: 10.1016/0029-554X(78)90832-7.
- [45] S. Gin, P. Frugier, P. Jollivet, F. Bruguier, et E. Curti, « New Insight into the Residual Rate of Borosilicate Glasses: Effect of S/V and Glass Composition », *Int. J. Appl. Glass Sci.*, vol. 4, n° 4, p. 371-382, oct. 2013, doi: 10.1111/ijag.12048.
- [46] R. Hellmann, « The albite-water system: Part IV. Diffusion modeling of leached and hydrogen-enriched layers », *Geochim. Cosmochim. Acta*, vol. 61, n° 8, p. 1595-1611, avr. 1997, doi: 10.1016/S0016-7037(97)00023-9.
- [47] S. Narayanasamy *et al.*, « Influence of composition of nuclear waste glasses on vapor phase hydration », *J. Nucl. Mater.*, vol. 525, p. 53-71, nov. 2019, doi: 10.1016/j.jnucmat.2019.07.015.
- [48] S. Narayanasamy, P. Jollivet, L. Sessegolo, F. Angeli, et A. Abdelouas, « Influence of temperature and relative humidity on vapor hydration of an AVM nuclear waste glass », *J. Nucl. Mater.*, vol. 543, p. 152571, janv. 2021, doi: <https://doi.org/10.1016/j.jnucmat.2020.152571>.
- [49] L. Gentaz, T. Lombardo, A. Chabas, C. Loisel, et A. Verney-Carron, « Impact of neocrystallisations on the SiO₂-K₂O-CaO glass degradation due to atmospheric dry depositions », *Atmos. Environ.*, vol. 55, p. 459-466, août 2012, doi: 10.1016/j.atmosenv.2012.03.008.
- [50] T. Lombardo *et al.*, « Characterisation of complex alteration layers in medieval glasses », *Corros. Sci.*, vol. 72, p. 10-19, juill. 2013, doi: 10.1016/j.corsci.2013.02.004.
- [51] L. Gentaz, T. Lombardo, C. Loisel, A. Chabas, et M. Vallotto, « Early stage of weathering of medieval-like potash-lime model glass: evaluation of key factors », *Environ. Sci. Pollut. Res. Int.*, vol. 18, n° 2, p. 291-300, févr. 2011, doi: 10.1007/s11356-010-0370-7.
- [52] R. Bouakkaz, « Altération aqueuse et hydratation en phase vapeur du verre SON68 à basse température (35-90°C) », Nantes, Ecole des Mines, 2014.
- [53] K. Cummings, W. A. Lanford, et M. Feldmann, « Weathering of glass in moist and polluted air », *Nucl. Instrum. Methods Phys. Res. Sect. B Beam Interact. Mater. At.*, vol. 136-138, n° Supplement C, p. 858-862, mars 1998, doi: 10.1016/S0168-583X(97)00758-1.
- [54] L. M. Anovitz, D. R. Cole, et M. Fayek, « Mechanisms of rhyolitic glass hydration below the glass transition », *Am. Mineral.*, vol. 93, n° 7, p. 1166-1178, juill. 2008, doi: 10.2138/am.2008.2516.
- [55] Y. Kudriavtsev, M. Avendano, G. Ramirez, et R. Asomoza-Palacio, « Water vapor interaction with borosilicate glass », *Solid State Ion.*, vol. 321, p. 122-125, 2018, doi: <https://doi.org/10.1016/j.ssi.2018.04.015>.
- [56] Y. Kudriavtsev, R. Asomoza-Palacio, et L. R. Manzanilla, « Interaction of Water Vapor with Silicate Glass Surfaces: Mass-Spectrometric Investigations », *Tech. Phys. Lett.*, vol. 43, p. 447-449, mai 2017, doi: DOI: 10.1134/S1063785017050054.
- [57] J. Neeway, « The alteration of the SON68 reference waste glass in silica saturated conditions and in the presence of water vapor », Université de Nantes, 2011.
- [58] S. Fearn, D. S. McPhail, R. J. H. Morris, et M. G. Dowsett, « Sodium and hydrogen analysis of room temperature glass corrosion using low energy Cs SIMS », *Appl. Surf. Sci.*, vol. 252, n° 19, p. 7070-7073, juill. 2006, doi: <https://doi.org/10.1016/j.apsusc.2006.02.101>.
- [59] R. K. Chinnam, P. C. M. Fossati, et W. E. Lee, « Degradation of partially immersed glass: A new perspective », *J. Nucl. Mater.*, vol. 503, p. 56-65, mai 2018, doi: 10.1016/j.jnucmat.2018.02.040.
- [60] N. Valle, « Traçage isotopique (²⁹Si et ¹⁸O) des mécanismes de l'altération du verre de confinement des déchets nucléaires : SON68 », Institut national polytechnique de Lorraine, 2000.
- [61] Houser, C. A., Herman, J.S., Tsong, I.S.T., White, W.B., et Lanford, W.A., « Sodium-hydrogen interdiffusion in sodium silicate glasses », *J. Non-Crystalline Solids*, vol. 41, p. 89-98, 1980.

- [62] K. Ferrand, A. Abdelouas, et B. Grambow, « Water diffusion in the simulated French nuclear waste glass SON 68 contacting silica rich solutions: Experimental and modeling », *J. Nucl. Mater.*, vol. 355, n° 1–3, p. 54–67, sept. 2006, doi: 10.1016/j.jnucmat.2006.04.005.
- [63] J.-C. Dran, J.-C. Petit, L. Trotignon, A. Paccagnella, et G. D. Mea, « Hydration Mechanisms of Silicate Glasses: Discussion of the Respective Role of ion Exchange and Water Permeation », *MRS Online Proc. Libr. Arch.*, vol. 127, ed 1988, doi: 10.1557/PROC-127-25.
- [64] L. T. Zhuravlev, « The surface chemistry of amorphous silica. Zhuravlev model », *Colloids Surf. Physicochem. Eng. Asp.*, vol. 173, n° 1, p. 1–38, nov. 2000, doi: 10.1016/S0927-7757(00)00556-2.
- [65] J. J. Mazer, C. M. Stevenson, W. L. Ebert, et J. K. Bates, « The Experimental Hydration of Obsidian as a Function of Relative Humidity and Temperature », *Am. Antiq.*, vol. 56, n° 3, p. 504–513, juill. 1991, doi: 10.2307/280898.
- [66] Y. Moriya et M. Nogami, « Hydration of silicate glass in steam atmosphere », *J. Non-Cryst. Solids*, vol. 38–39, p. 667–672, mai 1980, doi: 10.1016/0022-3093(80)90513-X.
- [67] A. Lasaga, *Rate laws of chemical reactions in Kinetics of Geochemical Processes*. Washington D.C.: A. C. Lasaga and R. J. Kirkpatrick, 1981.
- [68] C. Guy et J. Schott, « Kinetic Geochemistry Multisite surface reaction versus transport control during the hydrolysis of a complex oxide », *Chem. Geol.*, vol. 78, n° 3, p. 181–204, déc. 1989, doi: 10.1016/0009-2541(89)90057-0.
- [69] F. Alloteau, « Contribution à la compréhension des mécanismes de l'altération atmosphérique des verres et étude d'un traitement de protection à base de sels de zinc », phdthesis, PSL Research University, 2017.
- [70] R. Bouakkaz, « Altération aqueuse et hydratation en phase vapeur du verre SON68 à basse température (35-90°C) », Nantes, Ecole des Mines, 2014.
- [71] S. Brunauer, P. H. Emmett, et E. Teller, « Adsorption of Gases in Multimolecular Layers », *J. Am. Chem. Soc.*, vol. 60, n° 2, p. 309–319, févr. 1938, doi: 10.1021/ja01269a023.

Figure Captions

Fig. 1: SIMS elemental depth profiles of species present in SG3 glass reference (non-altered). The shaded part corresponds to the metallization of the sample (gold layer). For clarity purpose, the results were split onto two graphs a) and b).

Figure 2. Normalized SIMS profiles of a) 20-3m90%, b) 20-15m90% and c) 20-9mC. The horizontal dashed black line is an indication for the eye of normalized pristine content. The blue axis (right axis) refers to the D/H profiles. P and Mg profiles were not provided for 20-3m90%. The D/H profile on graph b) does not reach the value of 1 because the diffusion thickness of this element is 6 μm (see Fig. 10 for the entire profile). The shaded part on a) corresponds to the metallization of the sample.

Figure 3. Normalized SIMS profiles of the sample 50-4m55%. The horizontal black line at 1.0 is an indication for the eye of normalized pristine glass content.

Figure 4. XRD diffractograms of two samples and comparison with that of syngenite.

Figure 5. Raman spectra of two crystallized phases found on the surface of 20-9m40% and 20-9m90% (black and red curves, respectively, on the upper graph). Reference spectra of KNO_3 and CaCO_3 (from RRUFF database) are also presented (lower graph).

Figure 6. Optical images of the glass surfaces exposed for 4 months at 50°C at a) 95 %RH, b) 83 %RH, c) 76 %RH and d) 55 %RH. Images were taken after drying in desiccator. Samples were not washed.

Figure 7. SEM images (backscattered electron mode) of secondary phases at the sample surface exposed at 50°C 95% RH for 4 months. a) is the spectrum linked to b) and c) is the spectrum linked to d) More images and spectra are presented in the Supplementary material (Figure S1).

Figure 8. SIMS profiles of D/H for the samples exposed at 20°C for 9 months at several RH. b) Zoom of a) to observe the first peaks.

Figure 9. a) SIMS profiles of $^{18}\text{O}/^{16}\text{O}$ for the samples exposed at 20°C for 9 months at several RH. b) and c) correspond to the correlation of $^{18}\text{O}/^{16}\text{O}$ and D/H peaks (SIMS profiles) for 20-9m90%. c) is a window that targets the beginning of the curves. “ $^{18}\text{O}/^{16}\text{O}$ nat” and “D/H nat” corresponds to the ratio of natural abundances.

Figure 10. Normalized SIMS depth profiles of D/H for different exposure times at 90 %RH and 20°C.

Figure 11. Evolution of D/H SIMS depth profiles in the glass as a function of RH for samples exposed for 9 months at 20°C. “D/H nat” corresponds to the ratio of natural abundances.

Figure 12. (a) Normalized SIMS depth profiles of H/Si samples exposed at 50°C for 4 months at different RH. (b) is a window of the beginning of the curves in (a).

Fig. 13: Adjustments of deuterium SIMS diffusion profiles at 20°C with Fick and Doremus models. a, b) 20-3mC, c, d) 20-9mC e, f) 20-15m90%. Little boxes b, d and f) are the same curves in logarithm scale to better observe profiles.